Department of Physics and Astronomy
University of Heidelberg

Bachelor Thesis in Physics
submitted by

Charlotte Neitzel

born in Münster (Germany)

2017

Signal-Background Interference Pattern for Scalar Resonances

This Bachelor Thesis has been carried out by Charlotte Neitzel at the
Institute for Theoretical Physics in Heidelberg
under the supervision of
Prof. Dr. Tilman Plehn

Abstract

To discover or exclude at the LHC new particles, precise predictions of the expected kinematic patterns and cross sections are essential. In this thesis, we focus on the production of a heavy scalar singlet S through gluon fusion during 13 TeV LHC collisions and its decay into a pair of top-quarks ($gg \to S \to t\bar{t}$). We investigate systematically for which singlet scenarios the signal-background interference pattern contributes significantly to the signature of the scalar. To answer this question we will compute the partonic cross section of the signal process, of its interference with the background and of the background as well as simulate with MadGraph, for various scalar scenarios, the total and differential cross section of the different components during proton-proton collisions and analyze their dependences on the parameters of the scalar, including its mass, width, coupling constants and complex phase of the transition amplitudes.

We find that especially if the scalar has a large resonance width and weak scalar-gluon and scalar-quark couplings, the interference can be relevant and even dominant in the scalar signature. Depending on the complex phase of the signal and background transition amplitude, the interference can shift the invariant mass peak away from the resonance mass, or decrease (enhance) its counting rate as well as the total cross section. In some benchmark scenarios, the interference causes a dip below the continuum background which could not be detected when using the usual algorithm that only search for a peak.

Zusammenfassung

Um am LHC neue Teilchen zu entdecken oder auszuschließen, sind präzise Vorhersagen der nach Proton-Proton-Kollisionen zu erwartenden differentiellen und totalen Wirkungsquerschnitte notwendig. In dieser Arbeit untersuchen wir die Produktion eines schweren, skalaren Singuletts S durch Gluonenfusion während Proton-Proton-Kollisionen bei 13 TeV und seinen anschließendem Zerfall in ein Top-Antitop-Paar ($gg \to S \to t\bar{t}$). Ziel ist es, systematisch zu analysieren, für welche Szenarien die Interferenz zwischen Signal und Untergrund signifikant zu der Signatur des skalaren Teilchens beiträgt. Um diese Frage zu beantworten, werden wir sowohl analytische Berechnungen der partonischen Wirkungsquerschnitte von Signal, Interferenz und Untergrund durchführen als auch für verschiedne skalare Teilchen mit MadGraph die differentiellen und totalen hadronischen Wirkungsquerschnitte bei Protonen-Protonen-Kollisionen simulieren und deren Abhängigkeit von Parametern des Skalars, wie u.a. seiner Masse, Zerfallsbreite, Kopplungskonstaten sowie komplexen Phase der Amplitude, analysieren.

Unsere Ergebnisse zeigen, dass, insbesondere wenn das skalare Teilchen eine große Zerfallsbreite und geringe Kopplung an Gluonen und Quarks besitzt, die Interferenz einen relevanten und teils sogar dominanten Anteil an der Signatur des Skalars besitzt. Abhängig von der komplexen Phase der Signal- und Untergrundamplituden kann die Interferenz die Position der Resonanz verschieben oder die Zählrate dieser und somit den gesamten Wirkungsquerschnitt verringern bzw. erhöhen. Es lassen sich Beispiele finden, in denen dieses sogar zu einem Abfall der Zählrate unter die vom Standardmodell vorhergesagte Rate des Untergrunds führen kann und somit nicht durch die üblichen Algorithmen, die ausschließlich nach Peaks suchen, detektierbar ist.

Contents

1 Introduction and Motivation

The Standard Model (SM) of particle physics includes all so-far known fundamental particles and has been proven to describe a variety of the observed phenomena in particle physics. Despite the great success of the SM, there are still several remaining open questions. Phenomena like the nature of dark matter or the matter-antimatter asymmetry cannot yet be explained. Different theories have been developed in order to explain these 'beyond the Standard Model' (BSM) effects. The theories frequently predict new particles, which could be produced, for instance, in proton-proton (pp)-collisions at the Large Hadron Collider (LHC). The production amplitude for new particles at the LHC can interfere with SM amplitudes, leading to a shift in the expected event rates as well as characteristic patterns in the kinematic distributions.

In this thesis, we systematically analyze this interference effect in the production of a new scalar singlet particle decaying into a pair of top quarks $gg \to S \to t\bar{t}$. To obtain general results, we do not specify the model that predicts the scalar singlet further. We chose to investigate the production channel through gluon-fusion, because this is the channel with the largest production rate during pp-collisions. The amplitude from the scalar resonance interferes with the QCD continuum background process $gg \to t\bar{t}$. The total counting rate for all $gg \to t\bar{t}$ events includes signal events with an intermediate scalar, background events without intermediate scalar and the interference effects between signal and background. We aim to understand the structure of the interference term and its dependence on the different parameters such as the couplings, mass and total width of the new particle as well as the complex phases of the signal and background transition amplitudes. We tackle these questions with two tools: analytical calculations to help us understand the structure of the interference effects clearly, and Monte Carlo simulations with MadGraph [1] to include effects due to the parton distribution functions (PDF) and access different kinematic properties of simulated event samples.

So far, searches by the ATLAS and CMS experiments have not discovered any evidence of a new BSM scalar particle but set exclusion limits on the strength of the signal that a potential scalar can produce [2, 3]. However, current and future runs of the LHC will be sensitive to a much larger range of masses and couplings [4]. This will allow to detect rarer process and provides the potential to find new particles or set stronger exclusion limits. To assess if the measured data contain a new scalar, accurate predictions of the event rates are essential.

In contrast to previous analyses, the recent analysis by the ATLAS group [5] of data collected by the ATLAS experiment at the LHC, at an center-of-mass energy of $\sqrt{s} = 8\,\text{TeV}$, took interference effects into account. Former analyses have often only simulated the signal and the background but have neglected the interference.

Interference effects have been thoroughly studied in the literature. Many studies have focused on Higgs production in the $H \to \gamma\gamma$ channel [6, 7]. It has been shown that the interference between $H \to \gamma\gamma$ and the background can cause a shift of the diphoton mass peak [6]. Furthermore, the interference rate can be used to place limits or even measure the Higgs width [7].

Depending on the parameters of the new scalar, the shape of its interference distribution is comparable to the interference during a Higgs decay into photons. Similar to the $H \to \gamma\gamma$ interference, the $gg \to S \to t\bar{t}$ interference distribution consists of the real part of the interference amplitude, that has the shape of a bump and dip and is nearly anti-symmetric around the resonance mass and the imaginary part of the interference amplitude, which has the shape of a Breit-Wigner distribution with a negative (dip) sign [8, 9]. The relative importance of interference compared to the signal of the new scalar can be considerably larger than in the case of the interference of $H \to \gamma\gamma$ with the background. This is particularly true for a large scalar resonance width [10]. Thus, the interference term can overwhelm the perturbative peak of the resonance and lead to a peak-dip structure or even a dip alone, in the invariant mass distribution [8, 10]. In the following we want to answer the question for which parameters of the singlet scenarios the interference has a relevant influence on the line shape of the invariant mass distribution as well as on the total cross section.

This thesis is structured as follows: In the Sect. 2 we review some essential background information. This includes an introduction to the SM and its limits. We briefly discuss how new scalars can appear in extensions of the SM. We also discuss how such a new scalar particle could be produced and detected at the LHC.

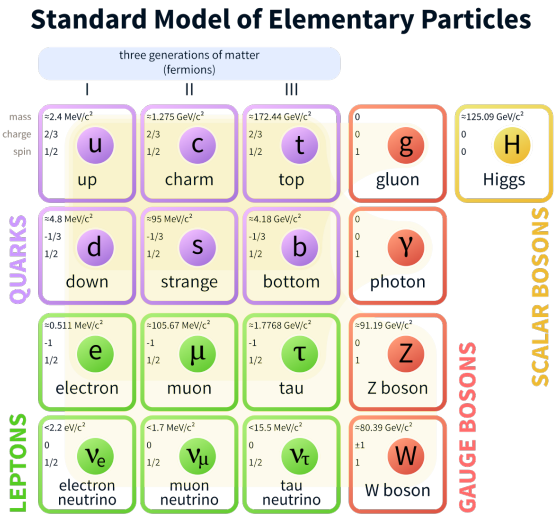

Figure 1: The Standard Model [11].

Sect. 3 provides a theoretical calculation of the partonic cross sections in presence of a scalar, for the general case with a pair of quarks in the final state. We calculate the partonic cross sections of the signal process ($gg \to S \to q\bar{q}$), the background process ($gg \to q\bar{q}$) and the interference between signal and background.

In the Sect. 4 we introduce numerical methods to generate and analyze signal, background and interference events of the process $gg \to q\bar{q}$ taking place during pp-collisions. Afterwards, in the Sect. 5, we present the results of simulations with a top quark pair in the final state, performed with the Monte-Carlo event generator MadGraph. We will discuss the dependence of the shape and the size of the differential cross sections on different parameters and compare the numerical results with the analytical results of Sect. 3. Furthermore, we discuss the influence of the quark mass on the cross sections and show results of simulations with a pair of bottom quarks in the final state.

Concluding remarks are made in Sect. 6.

2 Background

2.1 The Standard Model

The Standard Model is a fully renormalizable, Lorentz-invariant, gauge quantum field theory and includes the electroweak unification and QCD [12]. It not only classifies the elementary particles but also describes their fundamental interactions, except from gravity. The mass and kinetic terms of the particle fields of the SM, as well as the interaction terms, can be written down in a lagrangian. From this lagrangian, we can derive Feynman rules that can be used to calculate the probability of an interaction between particles of the SM [13].

We distinguish two groups of particles, fermions and bosons. Fermions have a non-integer spin and bosons have an integer spin. The group of fundamental, fermionic particles consists of spin-$\frac{1}{2}$ particles. These fermions can be can be subdivided into three generations of particles, where each generation contains two quark flavors and two leptons. The group of fundamental, bosonic particles consists of gauge bosons and the Higgs boson. Gauge bosons have spin-1 while the Higgs boson has spin 0. An overview of the SM particles is provided in Fig. 1. There are also antiparticles corresponding to the particles, that have opposite charge, flavour quantum-number and third component of the iso-spin, but the same mass. [12]

Leptons can be divided into two classes: leptons with the charge $e = -1.6 \times 10^{-19}\,\mathrm{C}$ and neutrinos (neutral leptons). Each generation of leptons contains one charged lepton and one

neutrino. The first generation consists of an electron and an electro-neutrino. The other two generations consist of one particle similar to the electron, but heavier, and its corresponding neutrino. Neutrinos are uncharged and predicted by the SM to be massless. [12]

Quarks are distinguished by their mass, their flavour and their electric and color charges. In each generation, there is one quark with charge $+2/3e$ and another quarks with charge $-1/3e$. The top quark is the heaviest quark. Quarks carry one of three possible colour charges. Due to the colour confinement, quarks cannot be observed individually. They have to form color-neutral particles called hadrons, consisting of a combination of two or three quarks. [12]

Gauge bosons mediate interactions between the different fermions. Charged particles can interact via the exchange of a photon (electromagnetic interaction). The weak interaction is mediated by $W^{\pm}$ and Z^0-bosons. Quarks interact by strong interaction via the exchange of gluons. There are eight differently colour-charged gluons, where each carries a combination of colour and anticolour. Different to photons, gluons interact with each other. [12]

The Higgs boson is the most recently discovered particle at the LHC. It is a scalar particle with no charge and mass $m_H = 125\,\text{GeV}$. It couples to particles via the Yukawa couplings. As the coupling strength is proportional to the particle mass, the particle with the largest coupling to the Higgs is the top quark. [14]

Even though the SM has predicted all so-far discovered fundamental particles and a variety of observed phenomena, it still has some deficiencies. For example, we can observe an oscillation between neutrinos of different generations, which is inconsistent with massless neutrinos. Furthermore, the nature of dark matter, dark energy and the matter-antimatter asymmetry cannot be explained by the SM. To explain these effects of so-called 'new physics', various new theoretical models have been developed [12]. Several of these models, especially the ones that aim to explain the nature of dark matter or the matter-antimatter asymmetry, include additional new scalar particles.

2.2 Higgs portal model

The simplest model including an additional scalar particle is the Higgs-portal model [15]. It extends the SM Higgs sector by adding a real scalar S_0 that transforms as singlet under the SM gauge group. The new scalar interacts with the other SM particles only by mixing with the SM Higgs doublet Φ_0. The Lagrangian of the Higgs sector is then given by

$$\mathcal{L}_{\text{Higgs}} = |D_\mu \Phi_0|^2 + |D_\mu S_0|^2 - \mu_1^2|\Phi_0|^2 - \lambda_1|\Phi_0|^4 - \mu_2^2|S_0|^2 - \lambda_2|S_0|^4 - \eta|\Phi_0|^2|S_0|^2, \tag{1}$$

where μ_i, λ_i are mass parameters and η defines the strength of the coupling [16]. We can rewrite the Lagrangian by expanding the two fields about their vacuum expectation $v_\Phi = (-\mu_1^2 - \eta v_S/2)/\lambda_1$ and $v_S = (-\mu_2^2 - \eta v_\Phi/2)/\lambda_2$, which gives us $\Phi_0 = (v_\Phi + \tilde{\Phi}_0)$ and $S_0 = (v_\Phi + \tilde{S}_0)$ [16]. The linear coupling between Φ_0 and S_0 induced by the term $\eta|\Phi_0|^2|S_0|^2$, leads to physical mass eigenstates that contain components of both fields. We obtain the mass eigenstates basis $\{S, \Phi\}$ by diagonalizing the Lagrangian, which gives us

$$\begin{pmatrix} \Phi \\ S \end{pmatrix} = \begin{pmatrix} \cos\alpha & \sin\alpha \\ -\sin\alpha & \cos\alpha \end{pmatrix} \begin{pmatrix} \tilde{\Phi}_0 \\ \tilde{S}_0 \end{pmatrix}, \tag{2}$$

where α is the mixing angle [16]. We can interpret the mass-eigenstate Φ as the Higgs boson with the mass $m_H = 125\,\text{GeV}$, which was discovered at the LHC [17]. The scalars Φ and S interact with fermions via Yukawa coupling of the doublet components. Thus, the interacting part of the lagrangian includes

$$\mathcal{L} \supset -y_f \tilde{\Phi}_0 \overline{f} f + \frac{g_{ggH}}{v_\Phi} \tilde{\Phi}_0 G^{\mu\nu} G_{\mu\nu} = -y_f \left(\cos\alpha\Phi - \sin\alpha S\right) \overline{f} f + \frac{g_{ggH}}{v_\Phi} \left(\cos\alpha\Phi - \sin\alpha S\right) G^{\mu\nu} G_{\mu\nu}, \tag{3}$$

where the second term of the lagrangian describes the effective coupling with the coupling constant g_{ggH} between gluon fields A_μ and the Higgs doublet using $G_{\mu\nu} = \partial_\mu A_\nu - \partial_\nu A_\mu + \mathcal{O}(A^2)$ [20]. The new scalar particle, S, interacts with fermions in the same way as the SM Higgs boson, but with

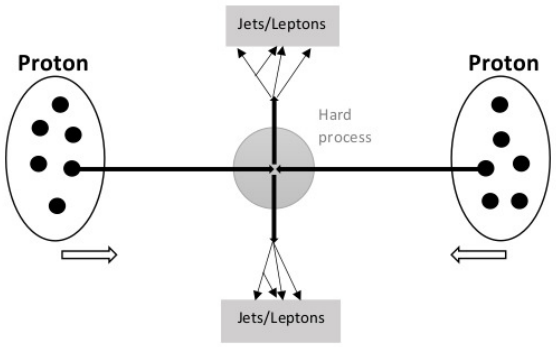

Figure 2: An example proton-proton collision at LHC.

differently-scaled coupling constants that depend on the mixing angle, α [18]. This simplified model requires further completion to render the scalar couplings gauge-invariant.

This model is just one of various possible models which includes an additional scalar. We will examine the interference between a scalar singlet and the SM background for the general case, not model specific. Consequently, we chose the singlet parameters, including the signal and background phases, the singlet mass, its width and the Scalar-quark/Scalar-gluon coupling to be independent of the limitations of a specific model.

2.3 LHC

The LHC is the biggest and most powerful particle accelerator worldwide [4]. Proton-proton (pp-) collisions are performed at high energy (currently up to 13 TeV [19]). Protons consist of partons, which are two up and one down valence quark and a sea of gluon and quarks/antiquarks of different flavours. The probability of finding a parton inside the proton, that has the momentum $x_i p$, where p is the momentum of the proton, is given by the PDF [20]. During a pp-collision the partons of the protons interact with each other ('hard process') [21]. Thereby, new particles, potentially including the new scalar S, could be produced as intermediate particles. The intermediate particles, produced in the collision, decay into final-state leptons or into gauge bosons and quarks that then decay further or hadronize. Because of the confinement quarks form jets consisting of highly boosted hadrons [20]. If during the 'hard-process' heavy particles like $W^{\pm}$ and Z^0 bosons or top quarks are produced, they decay further into leptons or into quarks that then form jets [21].

With the detectors at the LHC, particles like electrons, muons, photons, protons, neutrons and pions can be detected directly [21]. Furthermore, the initial state partons from the detected jets and its kinematic properties can be reconstructed using jet algorithms [20]. If the sum of the transverse momenta of the detected jets and leptons in the center of mass frame is non-zero, this can indicate the existence of a final state neutrino. We will discuss the detection methods that are relevant for our process further in Sect. 4.2.

The two biggest experiments at LHC are ATLAS and CMS [19]. Both experiments use general-purpose detectors that surround a pp-collision point. The number of pp-collisions at a given collision point per unit of time through unit transverse area is proportional to the luminosity, L, defined as

$$L \propto f n_1 n_2 / a, \tag{4}$$

where n_i is the number of particles per bunch, f is the crossing frequency and a the transverse profile of the beams [21].

So far, neither the data taken by ATLAS, nor by CMS has shown any hint for a new, BSM scalar particle [2, 3]. Consequently, if a new scalar particle exists, it must either have a very high mass and cannot be produced during the collisions at the LHC, or it has a very low cross section. In the case where the signal is too small to be distinguished from the background, it would be possible to discover the scalar with more data. Thus, the following data-taking periods, and especially the high-luminosity upgrade of the LHC in 2025, after which the LHC will have a 10 times higher

luminosity, provide possibilities to either discover a new scalar, if it exists, or to set new exclusion limits [22].

3 Analytical calculations

3.1 Calculating cross sections

To discover a new particle, it is necessary to predict its cross section. In order to get a first idea about how, in presence of a scalar, the events with a quark pair in the final state will be distributed in phase space, we begin by calculating the partonic cross section of the examined process. The cross section gives the likelihood of a particular final state for a given initial state [13]. It is not possible to calculate the hadronic cross section for a quark-pair final state during a pp collision analytically, because that requires including the parton distribution function of the protons (see Section 4.1). However, calculating the cross section at parton level will already give us a general idea of the line-shape of the hadronic differential cross section of the signal, interference and background and how they depend on the different parameters. In Sect. 5 we will find that most of the analytical calculated line shapes of the partonic cross sections as a function of the center of mass energy of the partons $\hat{s}$ are in good agreement with the line shapes of the differential hadronic cross sections as a function of $\hat{s}$,that we obtained when simulating pp-collisions numerically with MadGraph. Also, the observed dependence on the different parameters of the scalar was similar.

The differential cross section for a process with two colliding particles with momenta p_a and p_b and the energies E_a and E_b in the initial state and N particles with momenta $p_1, p_2, ..., p_N$ in the final state is given by

$$\mathrm{d}\hat{\sigma}(\hat{s}) = \frac{1}{(2E_a)(2E_b)|v_a - v_b|}|\mathcal{M}|^2 \mathrm{d}\Pi_{\mathrm{LIPS}}, \tag{5}$$

where $|v_a - v_b|$ is the relative velocity of the incoming particles and $\mathrm{d}\Pi_{\mathrm{LIPS}}$ is the Lorentz-invariant phase space [23]. The squared matrix element, $|\mathcal{M}|^2$, includes the average over initial states and the sum over final states spins and colours and is given by

$$|\mathcal{M}|^2 = |\langle f|\mathcal{M}|i\rangle|^2 = \frac{1}{n} \cdot \sum_{\text{polarization}} \sum_{\text{colors}} \left| \sum_{\text{diagrams}} \mathcal{M} \right|^2 , \tag{6}$$

where n is the number of possible initial states, $|i\rangle$ is the initial and $\langle f|$ the final state [23].

In the case of two-to-two particle scattering ($p_a p_b \to p_1 p_2$) in the center-of-mass frame, the cross section can be simplified to

$$\left(\frac{\mathrm{d}\hat{\sigma}}{\mathrm{d}\Omega}\right)_{\mathrm{CM}} (\hat{s}) = \frac{1}{64\pi^2 \hat{s}} \frac{|\vec{p}_1|}{|\vec{p}_a|} |\mathcal{M}|^2 \Theta(\sqrt{\hat{s} - m_1 - m_2}), \tag{7}$$

where $\sqrt{\hat{s}} = E_a + E_b = E_1 + E_2$ is the center-of-mass energy and Θ is the Heaviside function [23]. In the instance that the incoming particles are massless and the outgoing particles have equal masses $m = m_1 = m_2$, then the expression $\frac{|\vec{p}_1|}{|\vec{p}_a|}$ can be simplified to $\frac{|\vec{p}_1|}{|\vec{p}_a|} = \sqrt{1 - \frac{(2m)^2}{(p_a + p_b)^2}}$.

To calculate the squared matrix element we use Feynman rules. The Feynman rules for the scalar are obtained in analogy to the Feynman rules of the SM Higgs and can be found in Appendix A. We employ, as propagator of the scalar, a Breit-Wigner propagator

$$\frac{i}{(\hat{s} - m_s^2) + i m_s \Gamma_s}, \tag{8}$$

where Γ_s is the resonance width and m_s is the resonance mass.

3.2 Cross Section of $gg \to q\overline{q}$

The partonic cross section, $\hat{\sigma}$, of the process $g + g \to q + \overline{q}$ is given by

$$\hat{\sigma} \propto |\mathcal{M}_S + \mathcal{M}_B|^2 = |\mathcal{M}_S|^2 + 2\mathrm{Re}(\mathcal{M}_S^* \mathcal{M}_B) + |\mathcal{M}_B|^2 \propto \hat{\sigma}_S + \hat{\sigma}_i + \hat{\sigma}_B, \tag{9}$$

where $\mathcal{M}_S$ is the transition amplitude for quark pair production through an s-channel scalar, in a simplified model with effective gluon-scalar coupling (see Fig. 3), and $\mathcal{M}_B$ is the transition amplitude of the background, where no intermediate scalar is produced (see Fig. 4). In Fig. 3 and Fig. 4 the momenta of the incoming gluons are k_1 and k_2. The momenta of the outgoing quarks are p_1 and p_2. All momenta are defined in the center of mass system and from left to right in direction of the time axis.

For simplicity, from here on, 'signal' will refer to only the process where an intermediate scalar is produced ($gg \to S \to q\overline{q}$). Thus, the partonic cross section of the signal, $\hat{\sigma}_S$, is proportional to $|\mathcal{M}_S|^2$.

$$\text{'signal'} \propto \hat{\sigma_s} \propto |\mathcal{M}_S|^2. \tag{10}$$

The 'interference' is the part of the cross section that is proportional to $2\text{Re}(\mathcal{M}_S^* \mathcal{M}_B)$. Its partonic cross section is

$$\text{'interference'} \propto \hat{\sigma_i} \propto 2\text{Re}(\mathcal{M}_S^* \mathcal{M}_B). \tag{11}$$

We denote the part of the cross section that is different from the background, i.e. the sum of signal and interference as 'signal including the interference' , $\hat{\sigma}_{S+i} = \hat{\sigma}_i + \hat{\sigma}_S$. The 'background' is the process where no intermediate scalar is produced. Its partonic cross section, $\hat{\sigma}_B$, is proportional to $|\mathcal{M}_B|^2$.

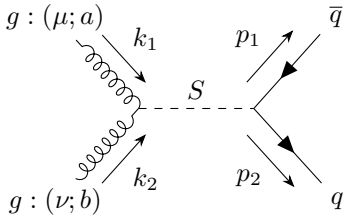

Figure 3: Feynman diagram of the signal process.

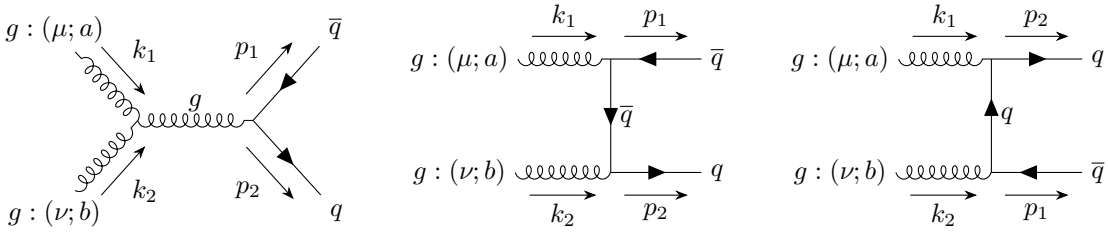

(a) Background term 1. (b) Background term 2. (c) Background term 3.

Figure 4: Feynman diagram of the background processes.

Using Feynman rules [13], we can derive the matrix element for the signal process

$$i\mathcal{M}_S = \epsilon_\mu^*(k_1) g_{gg}(-i)(k_{1,\nu}k_{2,\mu} - k_1 k_2 \eta^{\mu\nu})\epsilon_\nu^*(k_2) \frac{i}{((k_1+k_2)^2 - m_s^2) + i m_s \Gamma_s} \overline{u}(p_2)(i) g_{qq} v(p_1), \tag{12}$$

where $g_{gg} = |g_{gg}| \cdot e^{i\alpha}$ is the coupling constant between gluons and the scalar, $g_{qq} = |g_{qq}| \cdot e^{i\beta}$ is the coupling constant between the scalar and the quarks, $\eta^{\mu\nu}$ is the Minkowski metric and $\epsilon_\mu^*(k_1)$, $\epsilon_\nu^*(k_2)$ the polarization vectors of the initial state gluons.

The cross section of the signal is given by

$$\hat{\sigma}_s(\hat{s}) = \frac{\hat{s}^2}{256\pi} \left(1 - \frac{(2m_q)^2}{\hat{s}}\right)^{\frac{3}{2}} \frac{|g_{gg}|^2 |g_{qq}|^2}{(\hat{s} - m_s^2)^2 + (m_s \Gamma_s)^2} \Theta(\hat{s} - (2m_q)^2), \tag{13}$$

including the factor $\frac{1}{n} = \frac{1}{2\cdot 8}$, used for spin- and colour averaging. Gluons are colour octets that can have either a spin up or a spin down. Thus, there are $n = 8 \cdot 2$ possible initial states per gluon (8 possible colour states and 2 possible spin states). In the case of small quark masses, the partonic cross section calculated above of the signal Eq. (13) as a function of $\hat{s}$ is approximately a Breit-Wiegner distribution. Depending on the choice of parameters, the distribution is slightly asymmetrically shifted to larger $\hat{s}$ because of the $\left(1 - \frac{(2m_q)^2}{\hat{s}}\right)^{\frac{3}{2}}$ term. This effect is higher for larger Γ_s, because if the width is small, $\left(1 - \frac{(2m_q)^2}{\hat{s}}\right)^{\frac{3}{2}} \approx$ const. for $\sqrt{\hat{s}} \in [m_s - \Gamma_s, m_s + \Gamma_s]$. Furthermore, the shift due to $\left(1 - \frac{(2m_q)^2}{\hat{s}}\right)^{\frac{3}{2}}$ is higher for larger quark masses.

The matrix element for the first background diagram in Fig. 4a is given by

$$\begin{aligned} i\mathcal{M}_{B_1} =& \epsilon_\mu^*(k_1) g_s f_{abc} \left[(-2k_2 - k_1)^\nu \eta^{\mu\lambda} + (k_1 - k_2)^\lambda \eta^{\mu\nu} + (2k_2 + k_1)^\mu \eta^{\nu\lambda}\right] \\ & \epsilon_\nu^*(k_2) \frac{-i\eta_{\lambda\delta}\delta_{cd}}{(k_1 + k_2)^2} \overline{u}(p_2) i g_s T^d \gamma^\delta v(p_1), \end{aligned} \tag{14}$$

where g_s is the strong coupling constant. The matrix elements of the other two background diagrams, Fig. 4b and 4c, are given by

$$\begin{aligned} i\mathcal{M}_{B_2} + i\mathcal{M}_{B_3} =& \epsilon_\mu^*(k_1)\epsilon_\nu^*(k_2)\overline{u}(p_2)(ig_s)^2 \left[\gamma^\mu T^a T^b \frac{i(\not{k}_1 - \not{p}_1 + m_q)}{(p_1 - k_1)^2 - m_q^2}\gamma^\nu - \right. \\ & \left. \gamma^\nu T^b T^a \frac{i(\not{k}_2 - \not{p}_1 + m_q)}{(p_1 - k_2)^2 - m_q^2}\gamma^\mu\right] v(p_1). \end{aligned} \tag{15}$$

The differential cross section of the background process is given by

$$\begin{aligned} \frac{d\sigma_B}{d\hat{t}}(\hat{s}) =& \frac{g^4}{\pi 128 \hat{s}^2}\left[\frac{6(g_{qq}^2 - \hat{t})(m_q^2 - \hat{u})}{\hat{s}^2} - \frac{m_q^2(\hat{s} - 4m_q^2)}{3(m_q^2 - \hat{t})(m_q^2 - \hat{u})} + \frac{4(m_q^2 - \hat{t})(m_q^2 - \hat{u}) - 8m_q^2(m_q^2 + \hat{t})}{3(m_q^2 - \hat{t})^2}\right. \\ & \left. + (\hat{t} \leftrightarrow \hat{u}) - 3\frac{(m_q^2 - \hat{t})(m_q^2 - \hat{u}) + m_q^2(\hat{u} - \hat{t})}{\hat{s}(m_q^2 - \hat{t})} + (\hat{t} \leftrightarrow \hat{u})\right] \Theta\left(1 - \frac{(2m_q)^2}{\hat{s}}\right), \end{aligned} \tag{16}$$

where $\hat{t} = (p_1 - k_1)^2 = (p_2 - k_2)^2$ and $\hat{u} = (p_2 - k_1)^2 = (k_2 - p_1)^2$ are the Mandelstam variables [24].

The next step is to calculate the cross section for the interference term. As can be seen in Eq. (7), only the diagrams with the same initial state interfere with each other. To get a scalar particle, the spins and colors of the incoming/outgoing particles have to cancel each other [10]. This is not the case for the background diagram Fig. 4a, $gg \to g \to q\overline{q}$, because the propagating gluon has colour. Thus, there can only be an interference between the signal and the background diagrams Fig. 4b and Fig. 4c. The interference term is given by

$$\begin{aligned} \sum_{\text{polarization}} \sum_{\text{colors}} 2\text{Re}\left(\mathcal{M}_S^*(\mathcal{M}_{B_2} + \mathcal{M}_{B_3})\right) = 2\,\text{Re}\Bigg(& \sum_{\text{polarization}} \sum_{\text{colors}} \epsilon_\rho(k_1) g_{gg}^*(k_{1,\sigma}k_{2,\rho} - k_1 k_2 \eta^{\rho\sigma}) \\ & \epsilon_\sigma(k_2)\frac{-i}{((k_1 + k_2)^2 - m_s^2) - i m_s \Gamma_s}\overline{v}(p_1) g_{qq}^* u(p_2)\epsilon_\mu^*(k_1)\epsilon_\nu^*(k_2)\overline{u}(p_2)(ig_s)^2 \\ & \left[\gamma^\mu T^a T^b \frac{i(\not{k}_1 - \not{p}_1 + m_q)}{(p_1 - k_1)^2 - m_q^2}\gamma^\nu - \gamma^\nu T^b T^a \frac{i(\not{k}_2 - \not{p}_1 + m_q)}{(p_1 - k_2)^2 - m_q^2}\gamma^\mu\right] v(p_1)\Bigg). \end{aligned} \tag{17}$$

In the limit $m_q \to 0$, there is an odd number of γ matrices, so that the trace vanishes and the interference term is zero. Therefore, the interference term is enhanced by the mass of the quark. We can simplify the Eq. 17 by using

$$2\text{Re}\left(\frac{-g_{gg}^* g_{qq}^*}{(s - m_s^2) - i m_s \Gamma_s}\right) = \frac{2|g_{gg}||g_{bb}|}{(s - m_s^2)^2 + (m_s\Gamma_s)^2}\left(-\cos\phi(s - m_s^2) - \sin\phi m_s \Gamma_s\right), \tag{18}$$

where $\phi = \alpha + \beta - \xi$ is the difference between the strong phase of the signal $\alpha + \beta$ and the strong phase of the background ξ. The cross section of the interference term is then given by

$$\begin{aligned}\hat{\sigma}_{\mathrm{i}}(\hat{s}) =& \frac{1}{\pi \cdot 64\hat{s}} \frac{|g_{gg}||g_{bb}|}{(\hat{s}-m_s^2)^2+(m_s\Gamma_s)^2} \left(-\cos\phi(\hat{s}-m_s^2) - \sin\phi\, m_s\Gamma_s\right) g_s^2 m_q \\ & \left(\frac{-\frac{m_q^2}{2}(14\hat{t}+12\hat{u}) - \frac{3\hat{t}\hat{u}}{2} - \frac{\hat{t}^2}{2} - \hat{u}^2}{\hat{t}-m_q^2} - \frac{-\frac{m_q^2}{2}(14\hat{t}+12\hat{u}) - \frac{3\hat{t}\hat{u}}{2} - \frac{\hat{t}^2}{2}}{\hat{u}-m_q^2} \right) \\ =& \frac{1}{\pi \cdot 32} \frac{|g_{gg}||g_{bb}|}{(\hat{s}-m_s^2)^2+(m_s\Gamma_s)^2} \left(-\cos\phi(\hat{s}-m_s^2) - \sin\phi m_s\Gamma_s\right) g_s^2 m_q \\ & \left[\operatorname{artanh}\left(\sqrt{1-\frac{(2m_q)^2}{\hat{s}}}\right) - \sqrt{1-\frac{(2m_q)^2}{\hat{s}}} \right] \Theta\left(\hat{s}-(2m_q)^2\right). \end{aligned} \tag{19}$$

For $\phi = 0$ ($\phi = \pi$), the interference term Eq. (19) as a function of $\hat{s}$ has the shape of a peak followed by a dip (dip followed by a peak). For $\phi = \frac{\pi}{2}$ ($\phi = \frac{3\pi}{2}$) its shape is approximately a Breit-Wiegner distribution, but with a negative sign (positive sign). This will be discussed further in Sect 5.2, where we also show plots of the line shape of the partonic cross section for different phases (see Fig. 5).

3.3 Height (difference) of the peak (and dip) of $\hat{\sigma}(\hat{s})$

If we want to investigate how the size of the parton-level interference and signal terms are influenced by the choice of the couplings g_{gg}, g_{tt}, the width Γ_s, the scalar mass m_s and the quark mass m_q, there are two methods that we can choose. We can either discuss the influence on the total cross section, i.e. the integral of the cross section over $\hat{s}$, or look at the height (difference) of the peak (and dip), $\hat{A}$, of the partonic cross section defined as the difference between minimum and maximum of the partonic cross section:

$$\hat{A} = \hat{\sigma}_{\max}(\hat{s}_{\max}) - \hat{\sigma}_{\min}(\hat{s}_{\min}). \tag{20}$$

The total cross section is mainly influenced by the part of the interference-term proportional to $\sin\phi$, because the term proportional to $\cos\phi$ has a positive and a negative part that largely cancels in the total cross section. However, even for $\phi = 0$, the interference term can influence the kinematics, because it shifts the position of the maximum of the signal including the interference. This is why we choose to discuss the influence of the different parameter on $\hat{A}$.

As the partonic cross section of the signal is always positive and approaches zero for $\hat{s} \to \infty$. The height of the signal peak, $\hat{A}_s$, is given by $\hat{A}_s = \hat{\sigma}_{s,\max} - \hat{\sigma}_{s,\min} = \hat{\sigma}_{\mathrm{s},\max} - 0$. We can simplify the signal terms in Eq. (13), by expanding in a Taylor series around $\frac{(2m_q)^2}{\hat{s}} = 0$, which gives us

$$\begin{aligned}\hat{\sigma}_{\mathrm{s}}(\hat{s}) &= \frac{\hat{s}^2}{64^2\pi} \left(1-\frac{(2m_q)^2}{\hat{s}}\right)^{\frac{3}{2}} \frac{|g_{gg}|^2|g_{qq}|^2}{(\hat{s}-m_s^2)^2+(m_s\Gamma_s)^2} \Theta(\hat{s}-(2m_q)^2) \\ &= \frac{\hat{s}^2}{64^2\pi} \left(1-1.5\frac{(2m_q)^2}{\hat{s}}\right) \frac{|g_{gg}|^2|g_{qq}|^2}{(\hat{s}-m_s^2)^2+(m_s\Gamma_s)^2} \Theta(\hat{s}-(2m_q)^2) + \mathcal{O}\left(\left(\frac{4m_q^2}{\hat{s}}\right)^2\right). \end{aligned} \tag{21}$$

The maximum of the simplified term is at

$$\hat{s}_{\max} = m_s^2 + \Gamma_s^2 + O\left(\frac{4m_q^2}{\hat{s}}\right). \tag{22}$$

Evaluating Eq. (21) at $\hat{s}_{\max}$ gives us the height of the peak

$$\hat{A}_s = \hat{\sigma}_{s,\max} - 0 = \frac{|g_{gg}|^2|g_{qq}|^2}{4 \cdot 64^2\pi} \frac{m_s^2+\Gamma_s^2}{\Gamma_s^2} \left(1-1.5\frac{(2m_q)^2}{m_s^2+\Gamma_s^2}\right). \tag{23}$$

We find that, $\hat{A}_s$ is proportional to the squared coupling constants and in the case of $m_s \gg \Gamma_s$ and $m_s \gg m_q$, it is approximately proportional to $1/\Gamma_s^2$. Furthermore, $\hat{A}_s$ increases with m_s and decreasing with m_q.

Concerning the interference, there is no simple closed-form for the maximum and the minimum of the partonic interference cross section (Eq. (19)). To examine the dependence of the height (difference) of the peak (and dip) of the interference, $\hat{A}_i$, on Γ_s, m_s and ϕ, we have simplified the cross section further by approximating the interfering background near the resonance to be independent on $\hat{s}$ and using the narrow-width approximation (NWA). This is a reasonable approximation for very small Γ_s and should show schematically the dependence on the different parameters. Taking this into account and using that the transition amplitude of the signal is proportional to the propagator of the scalar multiplied with the coupling constants, we can simplify the interference term to

$$\begin{aligned}\hat{\sigma}_{\mathrm{i}} &\propto 2\mathrm{Re}\left(\mathcal{M}^*_{B_{2,3}} \frac{g_{gg} g_{qq}}{(\hat{s} - m_s^2) - i m_s \Gamma_s}\right) \\ &= |\mathcal{M}_{B_{2,3}}| \frac{2|g_{gg}||g_{qq}|}{(\hat{s} - m_s^2)^2 + (m_s\Gamma_s)^2} \left(-\cos(\phi)(\hat{s} - m_s^2) - \sin(\phi) m_s \Gamma_s\right),\end{aligned} \tag{24}$$

where $|\mathcal{M}_{B_{2,3}}|$ is the transition amplitude of the interfering part of the background.

For $\phi = 0$, the maximum and the minimum of the simplified interference term Eq. (24) differ only by sign and can be found at

$$\hat{s}_{\mathrm{min,max}} = m_s^2 \pm m_s \Gamma_s. \tag{25}$$

Thus, $\hat{A}_i$ of the $\phi = 0$ interference term is proportional to

$$\hat{A}_i \propto |\mathcal{M}_{B_{2,3}}| \frac{|g_{gg}||g_{bb}|}{m_s \Gamma_s}. \tag{26}$$

For $\phi = \frac{\pi}{2}$, the interference consists of only a peak with a maximum at $\hat{s}_{\mathrm{min/max}} = m_s^2$. Its height is the same as the height difference between peak and dip for $\phi = 0$.

We can conclude that $\hat{A}_i$ is approximately proportional to $1/\Gamma_s$ and proportional to g_{gg} and g_{qq}. The dependence on m_s is less obvious since the assumption that the background is the same for $\sqrt{\hat{s}} \approx 500\,\mathrm{GeV}$, which is approximately the position of the maximum for a singlet scenario with $m_s = 500\,\mathrm{GeV}$, as for $\sqrt{\hat{s}} \approx 1000\,\mathrm{GeV}$, which is approximately the position of the maximum for a singlet scenario with $m_s = 1000\,\mathrm{GeV}$, is not a good approximation. Thus, the decaying background has a non-negligible influence on the dependence of $\hat{A}_i$ on m_s, which can also be seen in Eq. (19) when evaluating the part of the cross section that is caused by the decaying background for large values of $\hat{s}$

$$\lim_{\hat{s}\to\infty} \left[\mathrm{artanh}\left(\sqrt{1 - \frac{(2m_q)^2}{\hat{s}}}\right) - \sqrt{1 - \frac{(2m_q)^2}{\hat{s}}}\right] = \infty. \tag{27}$$

If we compare $\hat{A}_s$ and $\hat{A}_i$, we observe that for sufficiently small $\frac{|g_{gg}||g_{qq}|}{\Gamma_s}$, $\hat{A}_i$ can be larger than $\hat{A}_s$. Thus, in this scenario, the interference becomes important for an accurate description of the process.

4 Numerical simulations

4.1 Simulations with Madgraph

After having calculated the partonic cross section for $gg \to q\overline{q}$ and discussed the influence of the different parameter, we want investigate which signal we would measure during pp-collisions at the LHC. To calculate such a hadronic cross section, we have to take into account the probability of finding a gluon i inside the proton, that carries the fraction x_i of the total proton momentum p. This probability is given by the PDFs $f_g(x_i)$; $f_g(x_i)$ decreases approximately with x_i^{-2} [20]. The hadronic cross section for obtaining a given final state during a pp-collision is given by

$$\sigma = \int dx_1 dx_2 \hat{\sigma}(\hat{s}) f_g(x_1) f_g(x_2) \delta(\hat{s} - x_1 x_2 s), \tag{28}$$

where s is the center of mass energy of the protons [21]. This integral has to be solved numerically, which is done by programs like Madgraph performing Monte-Carlo integration. Madgraph provides the total cross section, as well as event samples with kinematic features, mimicking measurable events. We will perform tree-level simulations with MadGraph Version 5 using the SM defined in FeynRules for background events and a self-implemented FeynRules model to generate events involving the scalar. We set the luminosity $\mathcal{L} = 300\,\text{fb}^{-1}$, the energy of the proton beams $\frac{\sqrt{s}}{2} = 6500\,\text{GeV}$ and the total number of events $N_{\text{total}} = 100000$. We used minimal phase-space cuts, including a minimal distance between jets of $\Delta R = 0.4$ [a], a maximum pseudorapidity of jets of $\eta = 5$, a minimum transverse momentum of jets of 20 GeV and a minimum invariant mass of b-quarks of $m_{bb,\text{min}} = 250\,\text{GeV}$.

4.2 Detection method

In Sect. 5.2-5.7 we will discuss the case where we have a top pair in the final state. This is the final state with the largest interference contribution.

Because of their short lifetime, we cannot detect top quarks directly. Almost 100% of the top quarks decay into a b-quark and a W^+ boson [26]. The $W^\pm$ bosons decay either leptonically or hadronically [26]. We want to look at the channel $t\bar{t} \to W^+bW^-\bar{b}$, where one $W^\pm$ boson decays leptonically and the other one hadronically ('lepton-plus-jets channel'), because this allows us to use the lepton as the trigger event [26]. Thus, we will detect events with one single muon or electron, missing transverse momentum which indicates the existence of the corresponding muon/electro-neutrino, two b-jet and other hadronic jets [27]. The hadronically decaying top quark (top quark that decays into the hadronically decaying $W^\pm$ boson) is reconstructed using top-tagging algorithm [28].

The branching ratio of the decay of the $W^\pm$ boson into hadrons is
$\text{Br}(W^\pm \to \text{hadrons}) = 67.42 \pm 0.27\%$ [26]. The branching ratio of the $W^\pm$-boson into electron is $\text{Br}(W^\pm \to e^\pm\nu) = 10.71 \pm 0.16\%$ and into muons is $\text{Br}(W^\pm \to \mu^\pm\nu) = 10.63 \pm 0.15\%$ [26]. Thus, the branching ratio for the decay of the top pair into the 'lepton-plus-jets channel' is given by $\text{Br}(t\bar{t} \to \text{lepton} + \text{jet}) = 2 \cdot 67.42\% \cdot 10.71\% \cdot 10.63\% = 28.89\%$, when using only electrons or muons as trigger events.

If we are looking at a real particle detector, we also need to take into account that not all of the decays of the top pair into 'lepton-plus-jets' events can be detected. The detection efficiency of the ATLAS detector for electrons and muons is about 90% [29, 27] . The b-tagging efficiency for the examined events is approximately 77% and the hadronically decaying top quark is detected with an efficiency of about 80% [27]. Thus, the total detection efficiency is approximately 55.44%. These efficiency values are only valid when performing various cuts on the data and using specific analyzing methods. To get an approximate idea of the counting rates, we will include these efficiency factors, even though we did not perform these cuts and analyzing methods in our simulations.

We will include the corresponding branching ratios and efficiencies in our analysis of data generated by MadGraph.

In Sect. 5.8 we will discuss the decay of the scalar into b-quarks. For the b-quark, the detection efficiency of the b-pair is 0.77^2. The $gg \to b\bar{b}$ process also has an additional, not interfering background component arising from $gg \to gg$ events, where the final state gluons are misidentified as pairs of b-quarks. As we mainly focus on the decay into a top pair final state and only provide approximate results for the b-quark final state, we will not take this extra background into account.

4.3 Analysis

We want to investigate the dependence of the interference and the signal terms on the complex phases of the signal and background transition amplitudes ϕ, the scalar mass m_s, the width Γ_s, the coupling constants g_{qq}, g_{gg} and the quark mass m_q. The relevant questions are how the kinematic distributions look, for which parameter values the interference term is negligibly small compared

[a] $\Delta R = \sqrt{\eta^2 + \Phi^2}$, where Φ is the azimuth angle around the beam pipe and $\eta = -\tan(\theta/2)$ is the pseudorapidity, defining θ as the polar angle [25].

to the signal and which parameters allow the interference and the signal to be distinguishable from the background. For various different parameters we will separately generate for the interference, signal and background event samples with MadGraph and plot histograms of the obtained the invariant mass distributions. The invariant mass distribution denotes the differential, hadronic cross section $\frac{\mathrm{d}\sigma}{\mathrm{d}m_{qq}}$ as a function of the invariant mass of the quark pair ($m_{qq} = \hat{s}$).

To observe the qualitative influence of the different parameters, we first show for several benchmark scenarios, histograms of invariant mass distribution. This allows us to observe the influence of the different parameters, not only on the size of the differential, hadronic cross sections, but also on the shape. We will compare the histograms of the invariant mass distributions obtained with MadGraph with the results of our analytical calculated parton-level cross section of Sect. 3.2.

Moreover, we want to take into account that the particle detectors do not measure the exact energy of the detected quarks. Real particle detectors have different energy resolutions and distributions in different parts of the detectors [6]. However, to show qualitatively the influence of the limited detector resolution, we approximate the measured energy to be a Gaussian distribution. A typical detector resolution in the search for new heavy resonance is 8% of the invariant mass of the top-pair (at $m_{tt} = 400\,\mathrm{GeV}$) [29]. Thus, to obtain plots including resolution effect, we produce a random, normally distributed number around the cm-energy m_{tt} with the standard deviation of 8% of m_{tt} of the event generated by MadGraph, and identify this number with the energy measured by the detector. We want to observe the effect of the energy resolution, depending on the shape of the histograms, which is influenced by the width Γ_s and the signal and background phases ϕ.

To quantify the effect of the different parameters on the size of the interference and signal terms, we plot the height (difference) of the peak (and dip) as a function of the different parameters. The height of the signal peak A_s and the height of the interference peak (and dip) A_i is defined as difference between the highest and lowest differential hadronic cross section per bin in the histogram. We will compare the numerically with MadGraph obtained dependence of A_s and A_i on the different parameters with the analytically in Sect. 3.3 calculated dependence of $\hat{A}_s$ and $\hat{A}_i$ on the different parameters.

To determine if the signatures of our singlet scenarios are actually relevant for LHC measurements and not just in the order of magnitude of statistical fluctuations of the background, we need to calculate their significance. In our analysis we will compute the significances over the QCD background on parton level of the signal alone, the interference alone, the absolute value of the interference alone and of the signal including the interference (i.e. the part of the total counting rate that is produced due to an intermediate scalar). If the significance of the signal including the interference is large enough, it is potentially possible to discover the scalar at the LHC. However, to perform precise predictions about the significance, we would need to discuss resolution effects and detection efficiency in more detail and perform further cuts on the data. As this is beyond the scope of this thesis, we will only roughly estimate the significance and discuss their dependence on different parameters.

We define the significance of the signal alone S_s, the significance of the interference alone S_i and the significance of the signal including the interference S_{s+i} as the sum of signal and/or interference events within a symmetric interval around the approximate position of the maximum of the signal divided by the statistical error of the background (the square-root of the sum of background-events within the same interval). For example, the significance of the signal including the interference is given by

$$\frac{\sum_{k=m_{\mathrm{qq,min}}}^{m_{\mathrm{qq,max}}} (\frac{\mathrm{d}\sigma_i^k}{\mathrm{d}m_{qq}} + \frac{\mathrm{d}\sigma_s^k}{\mathrm{d}m_{qq}})\mathcal{L}}{\sqrt{\sum_{k=m_{\mathrm{qq,min}}}^{m_{\mathrm{qq,max}}} \frac{\mathrm{d}\sigma_B^k}{\mathrm{d}m_{qq}}\mathcal{L}}}, \tag{29}$$

where $\mathcal{L}$ is the luminosity and thus $\frac{\mathrm{d}\sigma_x}{\mathrm{d}m_{qq}}\mathcal{L}$ the number of events per bin.

If we take into account resolution effects, an appropriate choice of the interval would be the position where the scalar is produced on-shell (i.e. at $\sqrt{\hat{s}} \approx m_s$) plus/minus its statistical error, which is given by the squared sum of the width Γ_s and the resolution of the detector. Assuming a

Table 1: Quantities characterizing the chosen singlet scenario. Can be evaluated separately $x \in \{$s (signal), i (interference), $|i|$, s+i (Signal including the interference), B (background), total (s+i+B)$\}$.

Symbol	Description	Expression	Sect.
$\hat{\sigma}_x(\hat{s})$	Partonic cross section of x	Calculated analytically	3.2
$\frac{\mathrm{d}\sigma_x}{\mathrm{d}m_{qq}}$	Differential cross Section of x during pp collision	Generated numerically with MadGraph	5
$\hat{A}_x$	Height (difference) of the peak (and dip) of $\hat{\sigma}_x(\hat{s})$	Calculated analytically from the function $\hat{\sigma}_x(\hat{s})$	3.3
A_x	Height (difference) of the peak (and dip) of $\frac{\mathrm{d}\sigma_x}{\mathrm{d}m_{qq}}$	Computed numerically from the histogram of $\frac{\mathrm{d}\sigma_x}{\mathrm{d}m_{qq}}$	5
S_x	Significance of x defined in Eq. (29)	Computed numerically from the histogram of $\frac{\mathrm{d}\sigma_x}{\mathrm{d}m_{qq}}$	5

detector with a energy resolution of the invariant mass of the top pair of 8% [29], we would obtain

$$m_{\mathrm{qq,min/max}} = m_s \pm \sqrt{\Gamma_s^2 + (0.08 \cdot m_s)^2}. \tag{30}$$

If we do not take into account resolution effects of the detector, then

$$m_{\mathrm{qq,min/max}} = m_s \pm \Gamma_s. \tag{31}$$

We did not take into account that the maximum is not at $\sqrt{\hat{s}} = m_s$, but slightly shifted due to phase space factors and PDF effects. However, this should not change our result significantly, because we choose a sufficiently large interval.

Table 1 shows an overview of the quantities that we want to analyze systematically for various different singlet scenarios. We will examine the dependence of the listed quantities as a function of each parameter of interest, namely the Signal and Background phases ϕ, the scalar mass m_s, the width Γ_s, the coupling constants g_{qq}, g_{gg} and the quark mass m_q.

4.4 Choice of parameter

While varying g_{tt}, g_{gg} and Γ_s, we have to make sure that the couplings of the new scalar S and its width Γ_s are chosen consistently. Equivalently, when we choose a given singlet scenario, the total decay width, Γ_s, has to be the sum of the partial widths, i.e.

$$\Gamma_s = \Gamma(S \to q\bar{q}) + \Gamma(S \to gg) + \Gamma(S \to x) > \Gamma(S \to q\bar{q}) + \Gamma(S \to gg), \tag{32}$$

where x are other particles like $W^\pm$ or Z^0 bosons that the scalar can decay into. In our simplified model we only consider the interaction between the scalar and gluons or quarks. Equivalently to condition that $\Gamma_s > \Gamma(S \to tt) + \Gamma(S \to gg)$, we can also assure that the sum of the branching ratios Br for a decay into tops and gluons

$$\mathrm{Br}(S \to tt) + \mathrm{Br}(S \to gg) = \frac{\Gamma(S \to tt)}{\Gamma_s} + \frac{\Gamma(S \to gg)}{\Gamma_s}, \tag{33}$$

must be < 1.

We can calculate the partial width $\Gamma(S \to tt)$ from the literature result for the SM Higgs boson,

$$\Gamma(H \to f\overline{f}) = N_c \frac{G_F}{4\sqrt{2}\pi} m_f^2 M_H \beta_f^3, \tag{34}$$

where $N_c = 3$ is the colour factor, m_f the fermion mass, M_H is the Higgs mass, $G_F = \frac{1}{\sqrt{2}v^2} = \frac{1}{\sqrt{2}(246\,\mathrm{GeV})^2}$ is the Fermi coupling constant and $\beta_f = \sqrt{1 - 4m_f^2/M_H^2}$ [30]. Thus, the branching ratio of our scalar particle is given by

$$\mathrm{Br}(S \to t\bar{t}) = \frac{\Gamma(H \to f\overline{f})}{\Gamma_s} \frac{g_{S\bar{q}q}^2}{g_{H\bar{q}q}^2} = \frac{3 m_s g_{qq}^2}{8\pi\Gamma_s} \beta_q^3, \tag{35}$$

where $g_{H\bar{q}q} = \frac{m_q}{v}$ is the coupling of the Higgs boson to a quark pair and $g_{S\bar{q}q}^2 = g_{qq}^2$ [8].

Values for the partial width $\Gamma(S \to gg)$ can be obtained, when simulating the decay of the scalar into gluons with MadGraph.

According to most models that predict the BSM scalar, the scalar particle should to have comparable properties and coupling constants as the Higgs boson. For example the Higgs portal model (see Section 2.2) predicts coupling constants smaller than the coupling constants of the Higgs boson. The effective coupling between Higgs and gluons is $g_{ggH} = \frac{\alpha_s}{v 12\pi} \approx 9.91 \times 10^{-6}\,\frac{1}{\mathrm{GeV}}$ [20]. The coupling between quarks and the Higgs is $g_{H\bar{q}q} = \frac{m_q}{v}$, which induces the coupling constant $g_{H\bar{t}t} \approx 0.84$ for top quarks and $g_{H\bar{b}b} \approx 0.13$ for bottom quarks [26].

For most simulations, if not specified otherwise, we choose $g_{gg} = 9.91 \times 10^{-6}\,\frac{1}{\mathrm{GeV}}$ and a value for g_{qq} that is around or lower the value of $g_{H\bar{q}q}$.

5 Physics questions

5.1 Overview

In this section we will present the results obtained with MadGraph. Apart from the simulations in Sect. 5.8, we investigate the process with a top pair final state because the interference is higher for a decay into a top pair, than for a decay into the other SM quarks (see Sect. 5.8). In Sect. 5.8, we will discuss the influence of the quark mass and perform simulations with a b-quark-pair in the final state.

Section 5 is organized as follows: in each subsection, we will discuss the dependence of the interference, signal and background on one of the parameters listed in Table 2. We will systematically vary the parameters in the region defined in Table 2 and choose the listed default values for the other parameters including $g_{gg} = \frac{\alpha_s}{12\pi v}$, $m_s = 500\,\mathrm{GeV}$, $\phi = 0$, and $\Gamma_s = 20\,\mathrm{GeV}$. In that case $\Gamma(S \to gg) \approx 0.8\,\mathrm{GeV}$. Apart from our scenarios in Sect. 5.7, we do not set the branching ratio $\mathrm{Br}(S \to \bar{t}t)$ to a fixed value but compute $\mathrm{Br}(S \to \bar{t}t)$ using Eq. (35) for each chosen singlet scenario. While varying the different parameters, we assure, that the branching ratio $\mathrm{Br}(S \to \bar{t}t)$ is ≤ 0.6 for all scenarios in the examined parameter range. The condition $\mathrm{Br}(S \to \bar{t}t) \leq 0.6$ leaves enough room to vary the parameters g_{tt}, Γ_s and m_s, that depend on the $\mathrm{Br}(S \to \bar{t}t)$, but also allows other decay channels. As we did not specified a model, we assume that for each given $\mathrm{Br}(S \to \bar{t}t)$ it is possible to find a model so that the sum over all branching ratios of the possible scalar-decays is 1.

We do not set a default value for g_{tt} but choose instead large values so that we obtain large signal and interference contributions (see Sect 5.5) but assure, that the condition $\mathrm{Br}(S \to \bar{t}t) \leq 0.6$ for all scenarios in the examined parameter range is full-filled and that g_{tt} is in the order of magnitude of g_{Htt}. However, as we are interested in observing generally the effect of a variation of the scalar parameters, the exact choice of the value of the different parameters is not that relevant. There are several benchmark scenarios in this section, where we did not used the default values but specified the chosen parameters.

To quantify the dependence of the interference, signal and background on the different parameters, we will plot histograms of differential cross sections with the bin size $\Delta m_{tt} = 1.6\,\mathrm{GeV}$ (if not specified differently) and then compute their height (difference) of the peak (and dip) A_s and A_i and significance S_s, S_i and S_{s+i} numerically for various of the in Table 2 listed singlet scenarios.

If we show histograms of benchmark invariant mass distributions, to demonstrate the influence of the different parameters (e.g. in Fig. 5, Fig 7, etc.), we use $g_{gg} = 1.3 \times 10^{-3}\,\frac{1}{\mathrm{GeV}}$ instead of the default value of g_{gg}. We are choosing a larger value of g_{gg}, because for the default parameters the background at $m_{tt} = 500\,\mathrm{GeV}$ is more than 500 times larger than A_i and A_s. The signal

Table 2: Overview of singlet parameters

Parameter	Symbol	Default	Investigated range	Sec.
Signal/background phase	ϕ	0 and $\frac{\pi}{2}$	$[0, 2\pi]$	5.2
Resonance mass	m_s	500 GeV	[500 GeV, 1000 GeV]	5.3
Resonance width	Γ_s	20 GeV	[5 GeV, 200 GeV]	5.4
Scalar-quark coupling	g_{tt}	none	$[0.1, 0.73]$	5.5
Scalar-gluon coupling	g_{gg}	$\frac{\alpha_s}{12\pi v}$	$[\frac{\alpha_s}{12\pi v}, 0.001\,\frac{1}{\text{GeV}}]$	5.6
Branching ratio	$\text{Br}(S \to \bar{t}t)$	≤ 0.6	$(0, 1)$	5.7
Quark mass	m_q	m_t	$[m_b = 4.2\,\text{GeV}, m_t = 172.4\,\text{GeV}]$	5.8

is proportional to g_{gg}^2 and the interference is proportional to g_{gg}. By choosing a larger value for g_{gg}, like for example $g_{gg} = 1.3 \times 10^{-3}\,\frac{1}{\text{GeV}}$, A_i and A_s can be in the order of magnitude of the background, which is a good benchmark scenario for showing histograms of the invariant mass distribution of signal and interference.

5.2 Signal and background phases

First, we analyze the dependence of the interference, signal and background on the complex phase ϕ of the signal and background matrix element.

Invariant mass distribution

In Section 3.2, we have calculated the cross sections for the signal and the interference at parton level. We found that the cross section of the signal and the background are independent of the phases but the shape of the partonic interference cross section, given in Eq. (19) crucially depends on ϕ between the signal and background matrix element:

$$\hat{\sigma}_i \propto \frac{-\cos(\phi)(\hat{s} - m_s^2) - \sin(\phi) m_s \Gamma_s}{(\hat{s} - m_s^2)^2 + (m_s \Gamma_s)^2}. \tag{36}$$

We demonstrate this dependence in Fig. 5 where we show the analytically calculated partonic cross section of the signal and the interference for $gg \to t\bar{t}$ as a function of the $t\bar{t}$ invariant mass for the singlet scenario $\Gamma_s/m_s = 0.04$, $S/B = 0.186$, $\text{Br}(S \to \bar{t}t) = 0.42$, $g_{gg} = 1.3 \times 10^{-3}\,\frac{1}{\text{GeV}}$ and $\phi = 0$ or $\phi = \frac{\pi}{2}$. We observe the Breit-Wigner shape of the signal component, which does not depend on any phases.

The real and imaginary parts of the interference term, corresponding to the first and second term in Eq. (19), predict strikingly different shapes. For a vanishing complex phase difference between the phases of the signal and background matrix element, $\phi = 0$ or $\phi = \pi$, we only see the real part of the interference, corresponding to a bump and dip, nearly anti-symmetric around the resonance mass (see Fig. 5a). On the other hand, relative phases $\phi = \frac{\pi}{2}$ or $\phi = \frac{3\pi}{2}$ only leave the imaginary part of the interference, described by a Breit-Wigner distribution with either a positive (bump) or negative (dip) sign (see Fig. 5b). Intermediate values of the relative phase lead to a superposition of these two distinct types of effects.

Even though our analytical calculations did not include PDF effects, the line-shape of the partonic cross sections as a function of $\hat{s}$ are similar to the invariant mass distributions of the differential hadronic cross section obtained with MadGraph (see Fig. 6). In Fig. 6, we have plotted histograms that show the over one bin integrated differential, hadronic cross section $\frac{\text{d}\sigma}{\text{d}m_{tt}}$ generated by Madgraph, as a function of the center of mass energy m_{tt} for different phases using the same singlet scenario as in the plot of the partonic cross sections in Fig. 5 (benchmark parameters: $\Gamma_s/m_s = 0.04$, $\text{Br}(S \to \bar{t}t) = 0.42$, $g_{gg} = 1.3 \times 10^{-3}\,\frac{1}{\text{GeV}}$). The distribution of the signal and the background components do not depend on ϕ. Given Eq. (13), the line shape of the signal is approximately a Breit-Wiegner distribution, which is in agreement with the numerical results. The distribution of the interference has the expected shape containing a peak (dip) followed by

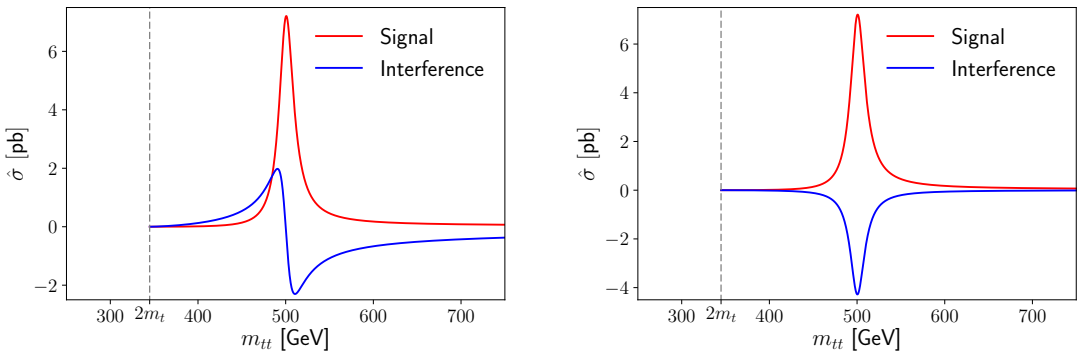

(a) $\phi = 0$. (b) $\phi = \frac{\pi}{2}$.

Figure 5: Calculated partonic cross section for the signal and interference component of $gg \to t\bar{t}$ as a function of the invariant mass of the top-pair $m_{tt} = \sqrt{\hat{s}}$. The singlet parameters are chosen as $\Gamma_s/m_s = 0.04$, $\mathrm{Br}(S \to \bar{t}t) = 0.04$, $g_{gg} = 1.3 \times 10^{-3} \frac{1}{\mathrm{GeV}}$, $m_s = 500\,\mathrm{GeV}$, $m_q = m_t = 172.4\,\mathrm{GeV}$, $g_{tt} = 0.19$. The signal component is shown in red, the interference is shown in blue.

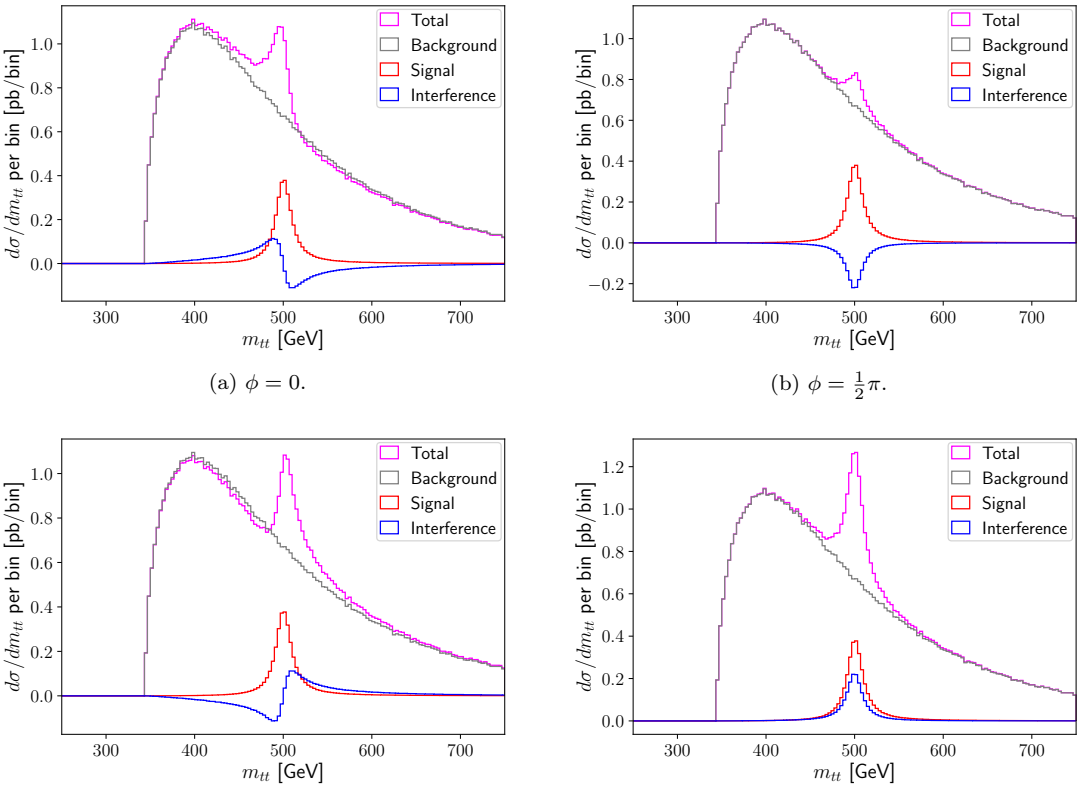

(a) $\phi = 0$. (b) $\phi = \frac{1}{2}\pi$.

(c) $\phi = \pi$. (d) $\phi = \frac{3}{2}\pi$.

Figure 6: Dependence of the invariant mass distribution generated by Madgraph on the phase ϕ. The singlet parameters are chosen as $\Gamma_s/m_s = 0.04$, $m_s = 500\,\mathrm{GeV}$, $g_{gg} = 1.3 \times 10^{-3} \frac{1}{\mathrm{GeV}}$, $g_{tt} = 0.19$ and $\mathrm{Br}(S \to \bar{t}t) = 0.04$. The total distribution is shown in magenta, the background distribution in grey, the signal distribution in red and the interference distribution in blue. Bin size: 3.3 GeV.

a dip (peak) for $\phi = 0$ ($\phi = \pi$). It is approximately a Breit-Wiegner distribution that interferes destructively (constructively) with the signal for $\phi = \frac{\pi}{2}$ ($\phi = \frac{3\pi}{2}$). For other phases it is a superposition of both shapes.

However, because of the phase-space factor $\sqrt{1 - \frac{(2m_q)^2}{m_{tt}^2}}$ in the partonic cross sections Eq. (19) and Eq. (13) (see Section 3.2), as well as PDF effects (see Sect. 4.1), both the signal and interference distributions are not completely symmetric around $m_{tt} = 500\,\text{GeV}$. The phase-space factors shift the distribution to larger energies whereas the PDFs, that describe that statistically gluons with a lower energy are preferred, shift the distribution to lower energies.

There are no signal, interference or background events for $m_{tt} < 2m_t = 345\,\text{GeV}$, because, in this case, the production of on-shell final state top quarks is not possible. The background is increasing fast in the energy region between $2m_t \leq m_{tt} \lesssim 400\,\text{GeV}$ and is decreasing slowly for higher energies.

In Fig. 7 we show the same histograms, also taking into account the smearing of the m_{tt} distributions due to the limited detector resolution. The dashed lines represent the signal that we would measure with a detector which has a Gaussian energy resolution of 8%. The 'measured' distributions are wider, but with lower A_i and A_s and the shape becomes more flattened out. The effect of the limited detector resolution is higher for $\phi = 0$ than for $\phi = \frac{\pi}{2}$. This is because the peak and the dip in the distribution with $\phi = 0$ are narrower and some of the negative events and the positive events cancel each other. Furthermore, when choosing $\phi = 0$ ($\phi = \pi$), the position of the peak/dip (dip/peak) is shifted by resolution effects to slightly lower/higher (higher/lower) energies then when not taking resolution effects into account.

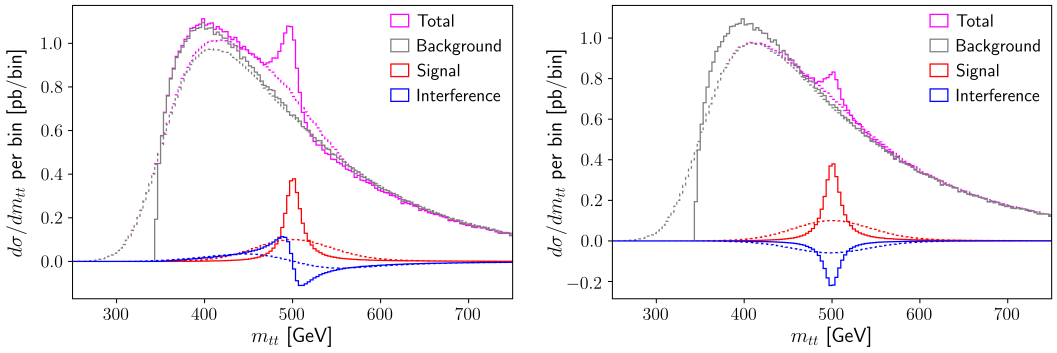

(a) $\phi = 0$. (b) $\phi = \frac{\pi}{2}$.

Figure 7: Resolution effects on the m_{tt} distribution. We show a singlet scenario with $\Gamma_s/m_s = 0.04$, $m_s = 500\,\text{GeV}$, $g_{gg} = 1.3 \times 10^{-3}\,\frac{1}{\text{GeV}}$, $g_{tt} = 0.19$ and $\text{Br}(S \to \bar{t}t) = 0.04$. The invariant mass distribution of the background is shown in grey, the signal distribution in red, the interference distribution in blue and the total distribution in magenta. The solid lines show the generated distributions and the dashed lines show the distributions including resolution effects. Bin size: 3.3 GeV.

In Fig. 6 and Fig. 7, we have chosen benchmark singlet scenarios with a scalar-gluon coupling of $g_{gg} = 1.3 \times 10^{-3}\,\frac{1}{\text{GeV}}$, that is around 130 times larger than the Higgs-gluon coupling. This large coupling constants are not typical for some models like the Higgs portal model. Fig. 8 shows the invariant mass distribution in a case with a gluon-Scalar coupling similar to the SM Higgs-scalar coupling ($g_{gg} = g_{ggH} = \frac{\alpha_s}{12\pi v}$, $g_{tt} = 3.626$, $\text{Br}(S \to \bar{t}t) = 0.6$, $\Gamma_s/m_s = 0.01$ and $\phi = \frac{\pi}{2}$). We observe that the interference term dominates over the signal component and thus, the singlet leads to a *dip* under the continuum background in the expected m_{tt} distribution rather than the usual excess of the background! To discover the scalar, we would need to search for a dip in the total counting rate, which would require a dedicated analysis method different from the usual bump hunting algorithms.

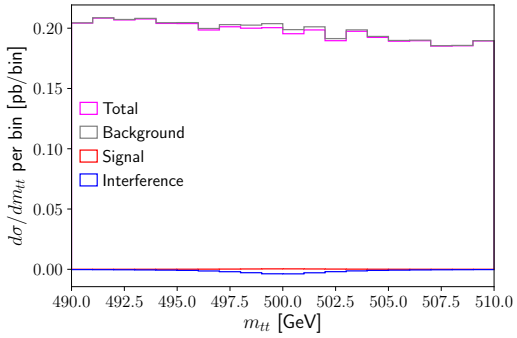

Figure 8: Invariant mass distribution generated by Madgraph for a singlet scenario with $g_{tt} = 3.626$, $\mathrm{Br}(S \to \bar{t}t) = 0.6$, $\Gamma_s/m_s = 0.01$, $m_s = 500\,\mathrm{GeV}$, $g_{gg} = \frac{\alpha_s}{12\pi v}$. The total distribution is shown in magenta, the background distribution in grey, the signal distribution in red and the interference distribution in blue. Bin size: 1 GeV.

Height (difference) of the peak (and dip)

Next, we want to quantify the effect of the phase on the size of the interference term. As described in Section 4.1.3, this can be done by plotting the height (difference) of the peak (and dip), defined as difference between the maximum and the minimum of the interference line shape, as a function of the phase.

Analytically, we did not find a simple closed-form of the height (difference) of the peak (and dip) of the interference cross section Eq. (19), $\hat{A}_i$, as a function of the phase. Instead, we numerically evaluate the cross section of the interference Eq. (13) for a large number of different $m_{tt} \in [250\,\mathrm{GeV}, 750\,\mathrm{GeV}]$ and then calculate the difference of the maximum and minimum value of the obtained array. We repeat this procedure for a large number of different phases and then plot the obtained $\hat{A}_i$ as a function of the phase. We find that the analytical calculated $\hat{A}_i$ is independent of the phase.

We have generated event samples with MadGraph for different phases ϕ using a singlet scenario with $g_{tt} = 3.626$, and otherwise the default parameter defined in Table 2 including $\Gamma_s/m_s = 0.04$, $\mathrm{Br}(S \to \bar{t}t) = 49\%$, $g_{gg} = \frac{\alpha_s}{12\pi v}$ and plotted histograms of the invariant mass distribution for each phase. From these histograms, we computed the height (difference) of the peak (and dip), A_i and A_s, and plotted them as a function of the phase (see Fig. 9). We find that A_i only slightly changes randomly with the phase. The position of the maximum/minimum of the invariant mass distribution and therefore also the position of the bin with the maximum/minimum differential cross section per bin changes with the phase. If the maximum/minimum of the differential cross section is at the border between two bin, we obtain a lower maximum/minimum differential cross section per bin and therefore lower values of A_i, than if the maximum/minimum is in the middle of a bin. This could cause the in Fig. 9 shown fluctuations of A_i. As the fluctuations are small, we can assume that the A_i is mostly independent of the phase which is in agreement with our results based on the analytically calculated cross section. Thus, we conclude that, in the following, when we are evaluating the dependence of A_i on the other parameters, it is sufficient to plot this dependence for only one fixed phase.

If the height of the signal peak A_s is equal to or greater than A_i, we would observe that the height (difference) of the peak (and dip) of the signal including the interference A_{s+i} is dependent on the phase. For our choice of parameters, that is not the case. Therefore, also the position of the maximum of the signal including the interference is at the position of the maximum of the interference. In Section 4.2.5, we describe how to choose the parameters such that the signal and the interference term have similar sizes. We will then also discuss the dependence of A_i and A_s and of the position of the maxima of the different terms on the phase in the case where the signal is larger than the interference.

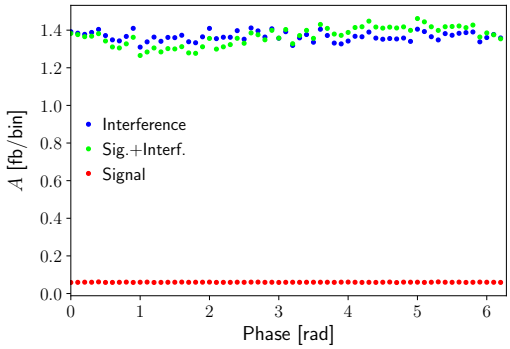

Figure 9: Height (difference) of the peak (and dip), A, of the signal distribution (red), the interference distribution (blue) and the signal including the interference distribution (green), obtained with Madgraph as a function of the phase. The singlet parameters are chosen as $\Gamma_s/m_s = 0.04$, $m_s = 500\,\text{GeV}$, $g_{tt} = 0.66$, $g_{gg} = \frac{\alpha_s}{12\pi v}$ and $\text{Br}(S \to \bar{t}t) = 49\%$. Bin size: 1.6 GeV.

Significance and total cross section

To determine if the signatures of our singlet benchmark scenarios are relevant for LHC measurements, we calculate significances as described in Sect. 4.3, both with and without detector resolution effects. We determine the significance over the QCD background of the signal alone, the signal including the interference, the interference term only, and the absolute value of the interference term only. We used the same singlet scenarios and generated data as when plotting A_i and A_s as a function of ϕ.

We have defined the significance of the signal and/or interference in Eq. (29) as the sum of signal and/or interference events within a symmetric interval around m_s, divided by the statistical error of the background (the square-root of the sum of background-events within the same interval). For $\phi = \frac{\pi}{2}$, the cross section of the interference is negative. Therefore, the contribution of the interference decreases the total counting rate, which is why the sum of the interference events, and thus its significance as defined in Eq. (29), is negative. From here on, significance, refers to the absolute value of the significance as defined in Eq. (29). For the significance of the interference it is possible that we obtain very low values because positive and negative values cancel each other when summing over the peak-dip shaped distribution. However, a peak-dip/dip-peak shaped interference distribution can have a considerable influence on the total distribution, for example by shifting its maximum to lower (larger) energies. Therefore, we not only plot the significance of the interference but also of the absolute values of the significance (i.e. we take the absolute value of each bin before summing over the given interval).

Fig. 10 shows that, as expected, the net effect of the interference on the event rate is small if the interference has a peak-dip/dip-peak-shape (i.e. for $\phi = 0$ and $\phi = \pi$) because the positive and negative events cancel each other, leading to very small values of the corresponding significance. The significance is maximal if the interference is a Breit-Wiegner distribution (for $\phi = \frac{\pi}{2}$ and $\phi = \frac{3\pi}{2}$). As described before, the effect of the limited detector resolution is higher for $\phi = 0$ and $\phi = \pi$, which is why the significance of the absolute value of the 'measured' interference term is lower for $\phi = 0$ and $\phi = \pi$.

In the parameter range we are looking at, the significance of the signal and the interference at $\phi = 0$ are negligible, but the significance of the absolute value of the interference term can be more than 5σ. For $\phi = \frac{\pi}{2}$ the significance of the sum of interference and signal distribution is above $5\,\sigma$. If the significance of the signal including the interference is high enough, it is potentially possible to discover the new scalar. However, a significance of 5σ at parton level does not necessarily mean that we will detect the singlet at the LHC. To perform predictions if a given singlet scenario would be observable in the distribution of detected events, we would need to include effects like detector simulations etc. in our simulation.

The described dependences can also be observed when looking at the total cross sections of

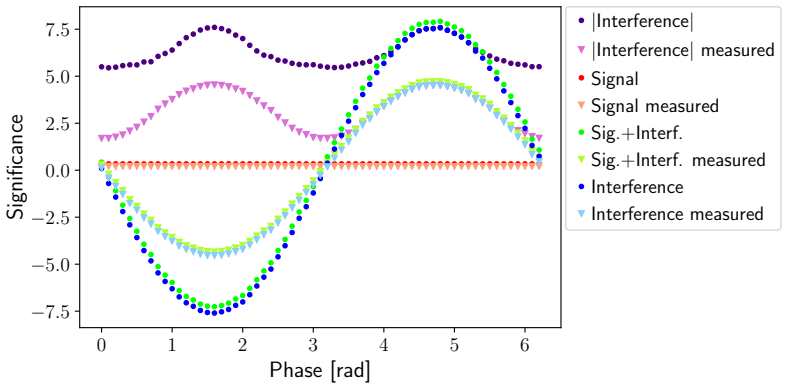

Figure 10: Dependence of the significance of the invariant mass distributions obtained with MadGraph on ϕ with and without resolution effects. We show a singlet scenario with $g_{tt} = 0.66$, $g_{gg} = \frac{\alpha_s}{12\pi v}$, $m_s = 500\,\text{GeV}$, $\text{Br}(S \to \bar{t}t) = 49\%$ and $\Gamma_s/m_s = 0.04$. The significance of the interference is shown in blue, the significance of the signal in red, the significance of the signal including the interference in green and the significance of the absolute values of the interference distribution in purple. The darker coloured dots show the significance of the generated distributions, the lighter coloured triangles show the significance of the distributions including resolution effects.

the described scenarios. The total cross section of the interference is $\sigma_{i,\text{tot}} = -0.05\,\text{pb}$ for $\phi = 0$, $\sigma_{i,\text{tot}} = -0.33\,\text{pb}$ for $\phi = \frac{\pi}{2}$. The total cross section of the signal is $\sigma_{s,\text{tot}} = 0.015\,\text{pb}$. The background with a total cross section of $\sigma_{B,\text{tot}} = 453.26\,\text{pb}$, and therefore largely dominating the signal and interference.

Summary

All in all, we observed that the phase of the signal and the background amplitude has a crucial influence on the shape of the interference distribution but no influence on the height (difference) of the peak (and dip), A_i, as well as on the signal and on the background. The results of the numerical simulation are in good agreement with our analytical results. We observed that the signal is Breit-Wiegner distributed and the interference has, depending on the phase, either an anti-symmetric bump-dip or dip-bump structure around the resonance mass, a Breit-Wigner-shaped bump or dip at the resonance mass, or a superposition of both. We have demonstrated that, for some parameter points, the interference term can dominate over the signal component. In these scenarios, the key signature of the scalar resonance can indeed consist of dips below the continuum background rather than the well-known Breit-Wigner peaks on top of it.

If we consider that the detector has a resolution of 8%, the line shape of the distributions is more flattened out. This effect is larger if the interference term has a peak-dip/dip-peak structure then if it only contains a dip/peak.

For the potentially possible choice of parameter that we used to plot the significances and the heights (differences) of peak (and dip), the interference was considerably larger than the signal. Thus, if such a scalar particle exists, the difference in the detected distribution of events to the expectations of the SM, would mainly be induced by interference effects. This can also be observed when plotting the significance of the sum of interference and signal depending on the phase. For our choice of parameters, the significance of the sum is larger than 5σ, for phases near $\phi = \frac{\pi}{2}$ and $\phi = 3\frac{\pi}{2}$ and negligible for phases near $\phi = 0$ and $\phi = \pi$ because when summing over the events, the positive and negative contributions cancel each other. Therefore, it is essential to include the interference in the analysis of experimental data. Analyzing methods that only search for a peak could, for example, not detect the case where $\phi = \frac{\pi}{2}$ and the total signal contains a dip. Even in the case where the interference term contains a peak it is important to include the structure of the interference in the analysis. For $\phi = 0$ the peak-dip structure of the interference shifts the position of the mass peak of the part of the signal differing from the background to considerably

lower energies.

5.3 Resonance mass

In this Section we examine the dependence of the interference and signal term on the scalar mass m_s.

Invariant mass distribution

Increasing m_s not only shifts the entire signal and interference distribution to larger energies but also has an influence on the height (difference) of their peaks (and dips) and their signficances. The analytically calculated cross section of the signal Eq. (13) is proportional to

$$\hat{\sigma}_s \propto \frac{1}{(\hat{s}-m_s^2)^2+(m_s\Gamma_s)^2}. \tag{37}$$

The analytically calculated cross section of the interference Eq. (19) is proportional to

$$\hat{\sigma}_i \propto \frac{-\cos(\phi)(\hat{s}-m_s^2)-\sin(\phi)m_s\Gamma_s}{(\hat{s}-m_s^2)^2+(m_s\Gamma_s)^2}. \tag{38}$$

Our analytical calculations of the partonic cross sections do not include PDF effects. If we vary the resonance mass over a wide range of energies, the influence of the PDFs is considerably large and thus we expect that our analytical results differ from the results we obtain numerically.

Height (difference) of the peak (and dip)

To quantify the effect of m_s on the size of the interference and signal term, we will investigate the height (difference) of the peak (and dip) of the signal and the interference. In Sect. 3.3, we found that the height of the signal-peak of the partonic cross section, $\hat{A}_s$, proportional to

$$\hat{A}_s \propto m_s^2+\Gamma_s^2-6m_q^2. \tag{39}$$

The analytically calculated height (difference) of the peak (and dip) of the interference Eq. (26), $\hat{A}_i$, does not have a realistic dependence on m_s, because the taken assumption of constant background does not hold when varying m_s over a large range of energies, as explained in Sect. 3.2. Thus, to plot the dependence of the analytical calculated cross section on m_s, we use the same method as in Sect. 5.2 to plot its dependence on the phase: We numerically calculate $\hat{A}_i$ of the partonic cross section Eq. (18) for a large number of m_s and then plot the dependence of $\hat{A}_i$ on m_s (see Fig. 11). We observe that $\hat{A}_i$ reaches a maximum and decreases afterwards. As described in Eq. (39), $\hat{A}_s$ increases with m_s^2.

In our numerical simulations with MadGraph, when we vary m_s between 500 GeV and 1 TeV for a singlet scenario with $\phi=\frac{\pi}{2}$, $g_{gg}=2\frac{\alpha_s}{12\pi v}$ and $\Gamma_s/m_s=0.04$, $g_{tt}=0.257$ and corresponding branching ratio $\mathrm{Br}(S\to t\bar{t})$ computed using Eq. (35), we observe that A_i decreases with m_s (see Fig. 12). For the signal we find that A_s increases until about $m_s=600\,\mathrm{GeV}$ and afterwards decreases with m_s. A_i and A_s approach each other with increasing m_s. However, for $m_s=1\,\mathrm{TeV}$, A_i is still 6 times higher than A_s.

The dependence of the with MadGraph obtained A_i and A_s on m_s differs from the analytically obtained dependence of $\hat{A}_i$ and $\hat{A}_s$ on m_s that based on the partonic cross sections. This can be justified by the fact that we did not included the PDFs in our analytical calculations. The, in the PDF defined probability of finding a gluon pair with a given energy m_{tt}, is lower for larger energies m_{tt}. Thus, if we would include the PDFs in the calculation of the cross section, this cross section would be lower for larger m_{tt} than the partonic cross section that we calculated analytically. An increasing m_s, shifts the position of the maximum/ minimum of the interference and the signal to larger m_{tt}. Thus, if we would include PDF effects, we would obtain significantly lower height (difference) of the peak (and dip) for larger m_s than the ones that we have calculated based on the partonic cross section.

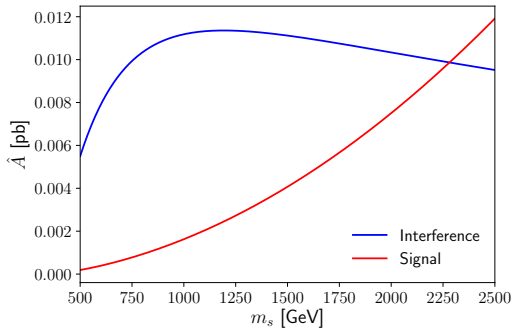

Figure 11: Calculated height (difference) of the peak (and dip) of the partonic cross section, $\hat{A}$, of the signal (red) and the interference (blue) as a function of m_s. The singlet parameter are chosen as $\phi = \frac{\pi}{2}$, $g_{gg} = 2\frac{\alpha_s}{12\pi v}$, $g_{tt} = 0.257$ and $\Gamma_s/m_s = 0.04$.

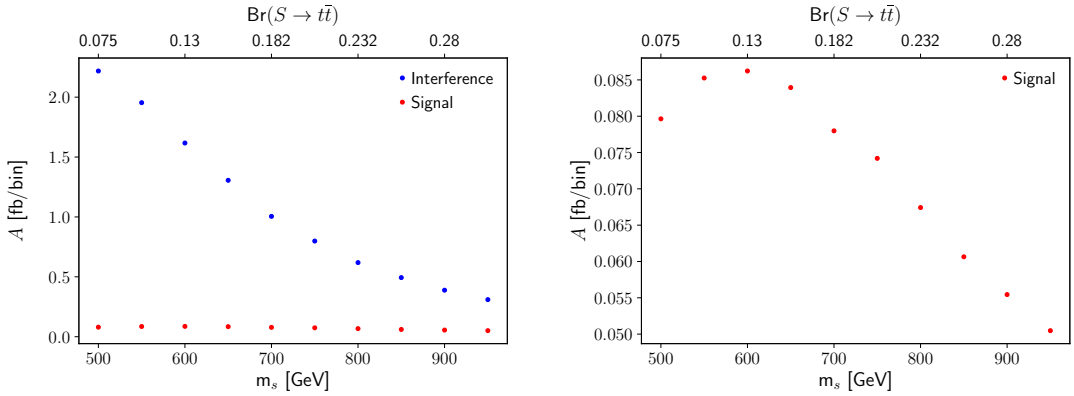

Figure 12: Height (difference) of the peak (and dip) of invariant mass distribution, A, of the signal (red) and the interference (blue) obtained with MadGraph as a function of m_s. The singlet parameter are chosen as $\phi = \frac{\pi}{2}$, $g_{gg} = 2\frac{\alpha_s}{12\pi v}$ and $\Gamma_s/m_s = 0.04$, $g_{tt} = 0.257$. The right figure is a zoomed in version of the left figure. Bin size: 1.6 GeV.

Significance

Fig. 13 shows the significance of the different components over the QCD background as a function of m_s. We used the same singlet scenarios and generated data as when plotting A_i and A_s. Unlike A_s, the significance of the signal increases with m_s (see Fig. 13). This is due to the fact that the background is lower at higher m_{tt}, so that the statistical error of the background is lower. This effect can also be observed when looking at the significance of the interference. The significance increases slightly for small m_s, but for larger m_s, the decrease in A_i is the dominating effect and thus the significance decreases. As we did not change Γ_s and g_{tt}, the branching ratio increases with m_s. If we leave $\mathrm{Br}(S \to \bar{t}t)$ fixed, we obtain higher significance of signal and of interference, when m_s is smaller than when $m_s = 1\,\mathrm{TeV}$.

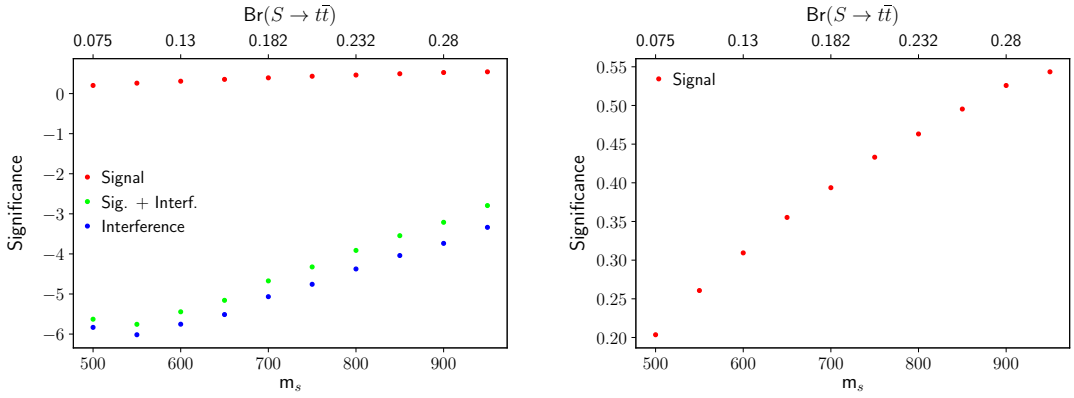

Figure 13: Dependence of the significance of the invariant mass distributions obtained with MadGraph on m_s. The singlet parameters are chosen as $\phi = \frac{\pi}{2}$, $g_{gg} = 2\frac{\alpha_s}{12\pi v}$, $\Gamma_s = 20\,\mathrm{GeV}$, $g_{tt} = 0.257$. The significance of the interference alone is shown in blue, the significance of the signal alone in red and the significance of the signal including the interference in green. The right figure is a zoomed in version of the left figure.

Summary

To summarize, we observed that both, the interference and the signal term are shifted to larger energies, when increasing m_s. The height (difference) of the peak (and dip) of the interference, A_i, decreases and the height of the signal-peak, A_s, first increases and then decreases with m_s. We obtain lower significances for the interference but larger significances for the signal when increasing m_s. The size of the signal and the interference are approaching with increasing m_s. To detect new scalar particles, which have very large masses m_s, we would need a higher energy regime than the current 13 TeV.

5.4 Resonance width

Next, we will observe the dependence of the signal and interference on the total resonance width Γ_s.

Invariant mass distribution

Examining the dependence on Γ_s is of interest, because Γ_s not only determines the width of the signal and interference distributions, but also has a large influence on their sizes relative to each other as well as compared to the background. This can be observed when analyzing the analytically calculated partonic cross sections, as well as when plotting the distributions obtained in our MadGraph simulation. The analytical partonic cross section of the signal (Eq. (13)) is

proportional to

$$\hat{\sigma}_s \propto \frac{1}{(\hat{s} - m_s^2)^2 + (m_s \Gamma_s)^2}. \tag{40}$$

The analytical partonic cross section of the interference (Eq. (19)) is proportional to

$$\hat{\sigma}_i \propto \frac{-\cos(\phi)(\hat{s} - m_s^2) - \sin(\phi) m_s \Gamma_s}{(\hat{s} - m_s^2)^2 + (m_s \Gamma_s)^2}. \tag{41}$$

Fig. 14 shows the numerical invariant mass distributions of the signal, background and interference for different $\Gamma_s = 30\,\text{GeV}$ and $\Gamma_s = 100\,\text{GeV}$. We chose as benchmark a singlet scenario with the coupling constant $g_{gg} = 1.3 \times 10^{-3}\,\frac{1}{\text{GeV}}$, $g_{tt} = 0.577$, $\phi = 0$ or $\phi = \frac{\pi}{2}$. We observe that, for larger Γ_s, the signal and the interference are wider but have a smaller size, which is in agreement with our expectations based on the partonic cross sections Eq. (19) and Eq. (13).

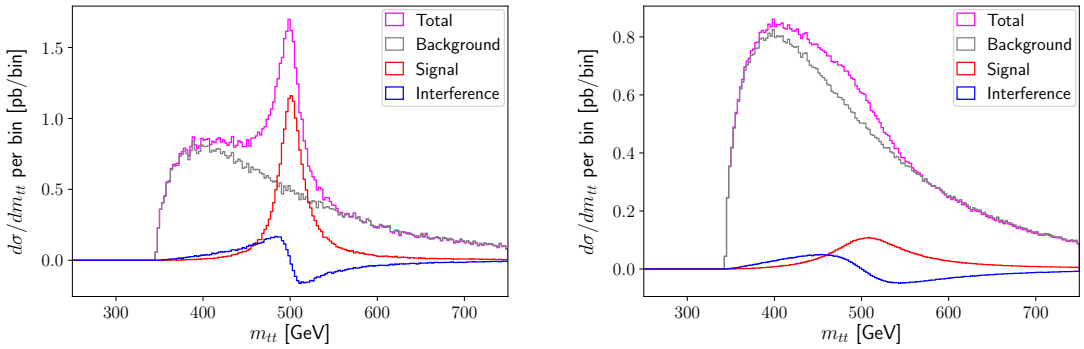

(a) $\Gamma_s/m_s = 0.06$, $\text{Br}(S \to \bar{t}t) = 0.36$, $\phi = 0$.

(b) $\Gamma_s/m_s = 0.2$, $\text{Br}(S \to \bar{t}t) = 0.073$, $\phi = 0$.

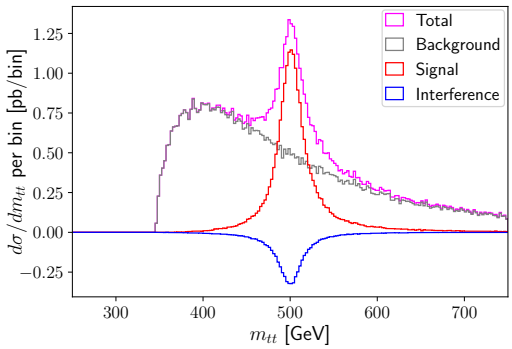

(c) $\Gamma_s/m_s = 0.06$, $\text{Br}(S \to \bar{t}t) = 0.36$, $\phi = \frac{\pi}{2}$.

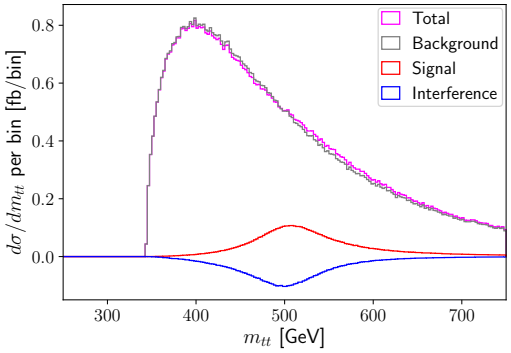

(d) $\Gamma_s/m_s = 0.2$, $\text{Br}(S \to \bar{t}t) = 0.073$, $\phi = \frac{\pi}{2}$.

Figure 14: Invariant mass distribution obtained with MadGraph depending on Γ_s/m_s. We choose a singlet scenario with $g_{gg} = 1.3 \times 10^{-3}\,\frac{1}{\text{GeV}}$, $m_s = 500\,\text{GeV}$ and $g_{tt} = 0.577$. The total distribution is shown in magenta, the background distribution in grey, the signal distribution in red and the interference distribution in blue. Bin size: 2.5 GeV.

If we take the energy resolution of the detector into account, we can observe that the smaller the value of Γ_s, the more the distribution of the signal and interference are influenced by resolution effects (see Fig. 15). This can be observed in Fig. 15, where we show the same histograms as 14a and 14b but with taking into account detector resolution effect.

Height (difference) of the peak (and dip)

To quantify the effect of Γ_s on the size of the signal and the interference, we determine the dependence of the height (difference) of the peak (and dip) on Γ_s.

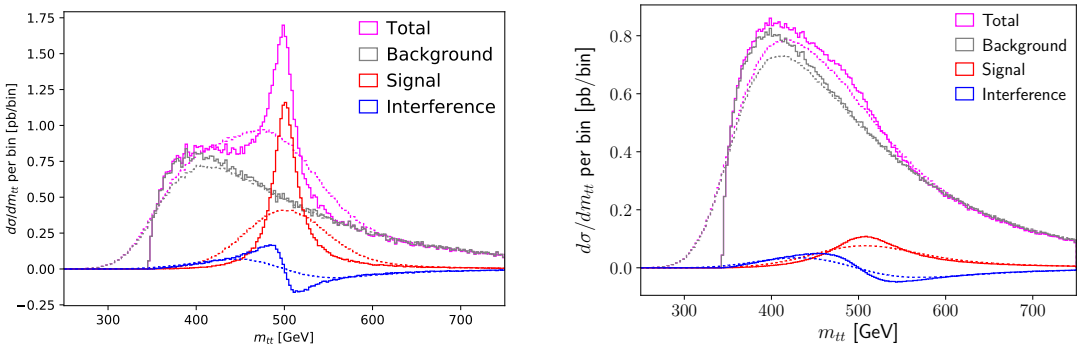

(a) $\Gamma_s/m_s = 0.06$, $\mathrm{Br}(S \to \bar{t}t) = 0.36$, $\phi = 0$.

(b) $\Gamma_s/m_s = 0.2$, $\mathrm{Br}(S \to \bar{t}t) = 0.073$, $\phi = 0$.

Figure 15: Invariant mass distribution for $\Gamma_s = 20\,\mathrm{GeV}$ and $\Gamma_s = 100\,\mathrm{GeV}$ including resolution effects of the detector. We choose a singlet scenario with $g_{gg} = 1.3 \times 10^{-3}\,\frac{1}{\mathrm{GeV}}$, $m_s = 500\,\mathrm{GeV}$ and $g_{tt} = 0.577$. The invariant mass distribution of the background is shown in grey, the signal distribution in red, the interference distribution in blue and the total distribution in magenta. The solid line show the distributions generated with MadGraph and the dashed lines show the same distributions but taking resolution effects into account. Bin size: 2.5 GeV

Analytically, we found in Section 3.3 that, in the case where m_q and Γ_s are small compared to m_s, the height of the signal peak of the calculated partonic cross section, $\hat{A}_s$, is proportional to

$$\hat{A}_s \propto \frac{1}{\Gamma_s^2} \tag{42}$$

and the height (difference) of the peak (and dip) of the calculated partonic cross section of the interference, $\hat{A}_i$, is proportional to

$$\hat{A}_i \propto \frac{1}{\Gamma_s}. \tag{43}$$

This is in good agreement with the results we obtain in our numerical simulation with MadGraph (see Fig. 16). Fig. 16 shows the height (difference) of the peak (and dip), A_i and A_s, in the invariant mass distributions generated with Madgraph as a function of Γ_s with and without detector resolution. We varied Γ_s between 5 GeV and 200 GeV and chose the default scalar-gluon coupling and scalar mass defined in table 2 ($g_{gg} = \frac{\alpha_s}{12\pi v}$, $m_s = 500\,\mathrm{GeV}$) and $g_{tt} \approx 0.363$. We compute the branching ratio $\mathrm{Br}(S \to t\bar{t})$ using Eq. (35) and obtained values between a few percent and around 60%. As A_i is independent of the signal and background phase ϕ (see Sect. 5.2), we only determine A_i for one benchmark phase ($\phi = 0$ here).

We observe that as expected from our analytical results, the numerically obtained values of A_s (A_i) are proportional to $1/\Gamma_s^2$ ($1/\Gamma_s$) and we can fit a $1/\Gamma_s^2$ ($1/\Gamma_s$)-function on the obtained values (see Fig. 16). As can be seen in Fig. 16, the background at $m_{tt} = 500\,\mathrm{GeV}$ is significantly larger than A_i and A_s. We would obtain a larger ratio between the signal/ interference and the background, when choosing lower values for Γ_s than the minimum value in Fig. 16 of $\Gamma_s = 5\,\mathrm{GeV}$. However, as explained in Sect. 4.4, if we want the coupling constant g_{tt} and the width Γ_s to be chosen consistently and equivalently that the branching ratio $\mathrm{Br}(S \to \bar{t}t)$, which is proportional to $\frac{g_{tt}^2}{\Gamma_s}$, is below 100%, we also need to choose a lower value of g_{tt}, when choosing a lower value of Γ_s. As the cross sections decrease with g_{tt}, this would cancel the effect of the increase of the ratio between the signal/ interference and the background due to the chosen lower value of Γ_s. In Section 4.2.6 we will further discuss what happens when we choose lower values of both Γ_s and g_{tt} and leave the branching ratio constant. Another possibility to obtain a larger ratio signal/interference to background is to choose a larger coupling constant g_{gg}. This will be discussed further in Sect. 5.6.

Furthermore, in Fig. 16, we show the A_i and A_s of the 'measured' distributions, which include the resolution effects of the detector. We find that A_i and A_s of the distributions that include

detector resolution effects are smaller than A_i and A_s of the distribution that do not include the limited detector resolution. We can confirm our observation based on the invariant mass distributions Fig. 15 that, the smaller the value of Γ_s, the larger the effect of the detector resolution.

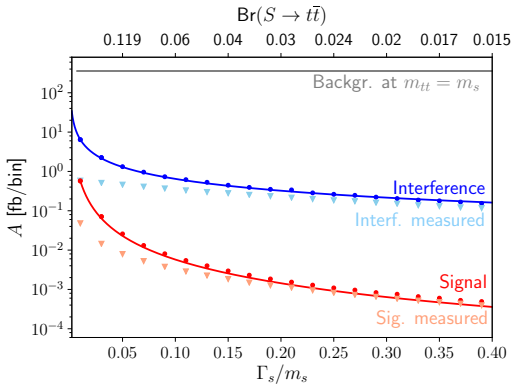

Figure 16: Height (difference) of the peak (and dip), A, of the signal distribution (red dots), the signal distribution including resolution effects (light red triangles), the interference distribution (blue dots) and the interference distribution including resolution effects (light blue triangles) depending on Γ_s/m_s. We choose a singlet scenario with $\phi = 0$, $g_{gg} = \frac{\alpha_s}{12\pi v}$, $m_s = 500\,\text{GeV}$ and $g_{tt} = 0.36$. The solid grey line shows the cross section of the background in the bin at $\sqrt{\hat{s}} = 500\,\text{GeV}$. The red (blue) solid line shows function $1/\Gamma_s^2$ ($1/\Gamma_s$) fitted on the height (difference) of the peak (and dip). Bin size: 1.6 GeV.

Position of the resonance maximum

Next, we want to discuss the influence of Γ_s on the position of the maximum of the invariant mass distribution of signal only, interference only and signal including the interference.

In Section 3.3 we found that the position of the maximum of the partonic cross section of the signal Eq. (22) is at $\hat{s}_{\text{max,s}} = m_s^2 - \Gamma_s^2$. The computed maximum of the partonic cross section of the interference Eq. (25) for $\phi = 0$ is approximately at $\hat{s}_{\text{max,i}} = m_s^2 - m_s\Gamma_s$. As we used various approximations and simplifications while calculating the position of the maxima, these positions differ from the position of the maxima of the partonic cross sections, which we would obtain without performing any approximations. This holds especially for larger Γ_s, where the approximation of having a constant background is no longer valid. Thus, we evaluated the partonic cross sections (Eq. (19) and (13)) for a large number of $\sqrt{\hat{s}} \in [250\,\text{GeV}, 750\,\text{GeV}]$ and calculated and plotted the position of the maxima for different Γ_s (see Fig. 17, straight lines). We observe that the position of the maximum of the signal is shifted to larger energies with increasing Γ_s, which can be explained by phase space factors. The position of the maximum of the peak-dip shaped interference is shifted to lower energies with increasing Γ_s because the distribution is becoming wider with Γ_s.

This general behaviour is in agreement with the results of our numerical simulations (see Fig. 17). The dots plotted in Fig. 17 show the position of the maximum of the signal and the interference as a function of Γ_s using the same generated data as when plotting A_i and A_s. As the height ot the signal peak is distinctly lower than the height the interference peak, the position of the maximum of the signal including the interference coincides with the position of the maximum of the interference.

We can observe in Fig. 17 that the positions of the maxima in the histograms obtained with Madgraph do not completely coincide with the results of our analytical simulations. This is because we did not included the PDFs in our analytical calculations. Statistically, gluons with lower momenta are preferred. This increases the differential cross section at lower energies and thus also shifts the maximum to lower energies.

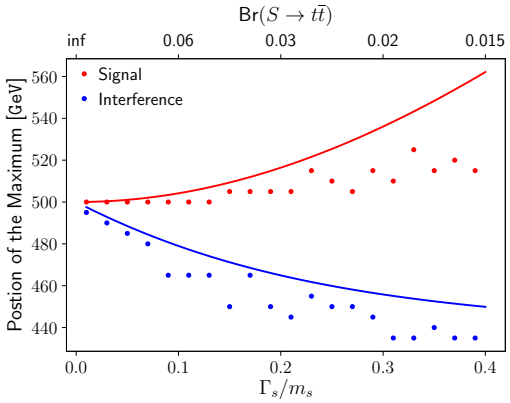

Figure 17: Position of the maxima of the signal only (red dots) and the interference only (blue dots) as a function of Γ_s/m_s. We choose a singlet scenario with a $g_{gg} = \frac{\alpha_s}{12\pi v}$, $g_{tt} = 0.36$, $m_s = 500\,\text{GeV}$ and $\phi = 0$. The position of the maximum of the interference only coincides with the position of the maximum of the signal including the interference. The red/blue lines show the calculated position of the maxima of the partonic cross sections of the signal/interference.

Significances

Next, we want to investigate the influence of the resonance width on the statistical significance of the different components. As A_i and A_s decreases with Γ_s, we expect that the significance of the signal and the absolute values of the interference also decreases with Γ_s. This can indeed be observed in Fig. 18, where we plot the significances of the interference, the signal and the signal including the interference over the QCD background as a function of Γ_s using the same data as when plotting A_i and A_s as a function of Γ_s.

In our chosen benchmark scenario, the significances of both, the signal and the interference for $\phi = 0$ are negligible. Only for small Γ_s/m_s the significances of the absolute value of the interference, and in a singlet scenario with $\phi = \frac{\pi}{2}$ also of the interference alone and the signal including the interference, are larger than 5σ. For $\phi = 0$ the significance of the interference term fluctuates around zero from $\Gamma_s/m_s = 0.01$ until $\Gamma_s/m_s = 0.2$ and decreases thereafter (see Fig. 18). This can be explained by the fact that for small Γ_s the interference term contains approximately as many positive as negative events. However, the cross section decreases to zero if m_{tt} is below the top quark threshold $2m_t$ (see Fig. 14). Thus, if Γ_s is of the size $m_s - 2m_t$ or larger, the top-production threshold lies inside the interval $[m_s - \Gamma_s, m_s + \Gamma_s]$, over that we are integrating the differential cross section to compute the significance (as defined in eq. (29)). The differential cross section within that interval is no longer anti-symmetric around the resonance mass and the integral is no longer vanishing, wherefore we obtain negative values for the significance of the bump-dip shaped interference term.

The significances of the signal and/or interference are smaller, when taking into account the limited detector resolution. This effect is more distinctive for smaller Γ_s.

Summary

We found that the shape of distribution of the signal and interference are wider but of smaller size when Γ_s is larger. The larger Γ_s, the smaller the effect of the limited detector resolution on the shape of the kinematic distribution. The height (difference) of the peak (and dip) of the interference distribution, A_i, is proportional to $\frac{1}{\Gamma_s}$ and the height of the peak of the signal distribution, A_s, is proportional to $\frac{1}{\Gamma_s^2}$. Thus, the ratio of the interference to signal is proportional to Γ_s. For our choice of parameters, the interference is larger than the signal but small compared to the background. The position of the maximum of the signal is shifted to larger energies with increasing Γ_s while the position of the peak in the peak-dip-shaped interference distribution is shifted to lower energies. The significance of the signal and interference both decrease with increasing Γ_s. However, the

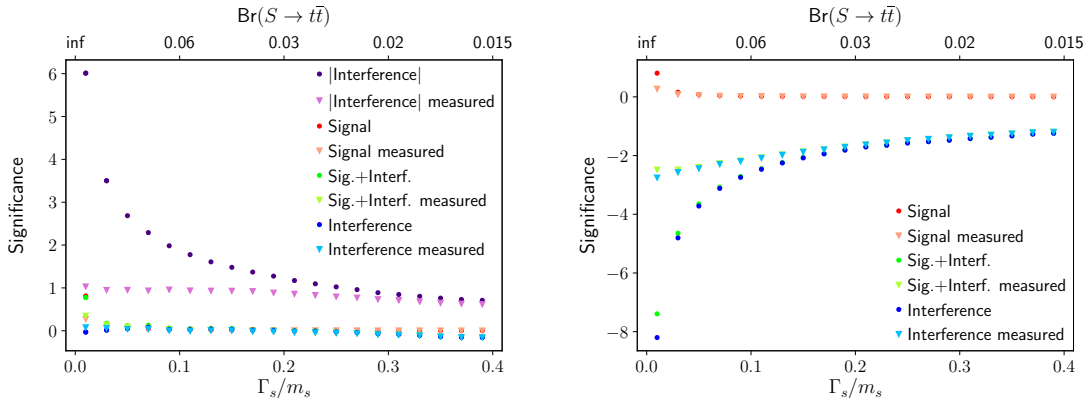

(a) $\phi = 0$.

(b) $\phi = \frac{\pi}{2}$

Figure 18: Dependence of the significance over the QCD background on Γ_s/m_s. We show singlet scenarios with $g_{gg} = \frac{\alpha_s}{12\pi v}$, $m_s = 500\,\text{GeV}$ and $g_{tt} = 0.36$. The significance of the interference over the QCD background is shown in blue, the significance of the signal only in red, the significance only of the signal including the interference in green and in the left Figure the significance of the absolute values of the interference distribution is shown in purple. The darker coloured dots belong to the significance of the distributions generated with MadGraph, the lighter coloured triangles to the significance of the distributions generated with MadGraph including resolution effects.

significance of the signal and of the interference for $\phi = 0$ are both negligible but the significance of the absolute value of the interference and of the interference for $\phi = \frac{\pi}{2}$ are both larger than 5σ for small Γ_s.

5.5 Scalar-quark coupling

In this Section we discuss the influence of the scalar-top coupling, g_{tt}, on the interference and the signal.

Invariant mass distribution and Signal to Background ratio

In our analytical calculations we found that

$$\hat{\sigma}_s \propto g_{tt}^2, \tag{44}$$

(see Eq. (13)) and that

$$\hat{\sigma}_i \propto g_{tt}, \tag{45}$$

(see Eq. (19)).

We observe as analytically predicted that, when generating kinematic distributions with MadGraph, both the signal and interference increase with g_{tt} but do not change in shape (see Fig. 19). Fig. 19 shows the kinematic distribution for singlet scenarios with the benchmark parameter $\Gamma_s/m_s = 20\,\text{GeV}$ and $g_{gg} = 1.3 \times 10^{-3}\,\frac{1}{\text{GeV}}$ and $g_{tt} = 0.077$ or $g_{tt} = 0.23$.

Thus, the only observables that are influenced by g_{tt} are the ratio 'signal including interference to background' (S/B). We can define the ratio S/B as

$$S/B = \frac{\sum_{k=m_{\text{tt,min}}}^{m_{\text{tt,max}}} \frac{\mathrm{d}\sigma_i^k}{\mathrm{d}m_{tt}} + \frac{\mathrm{d}\sigma_s^k}{\mathrm{d}m_{qq}}}{\sum_{k=m_{\text{tt,min}}}^{m_{\text{tt,max}}} \frac{\mathrm{d}\sigma_B^k}{\mathrm{d}m_{tt}}}, \tag{46}$$

with $m_{\text{tt,xmin/max}} = 500\,\text{GeV} \pm \Gamma_s$ (using the same $m_{\text{tt,xmin/max}}$ as for the significance in Eq. (30)). From our analytical calculation (Eq. (13)), we expect that, if the signal dominates the interference

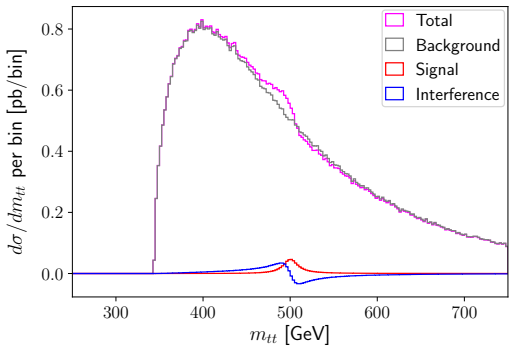

(a) $\mathrm{Br}(S \to \bar{t}t) = 0.0067$, $\phi = 0$, , $g_{tt} = 0.077$.

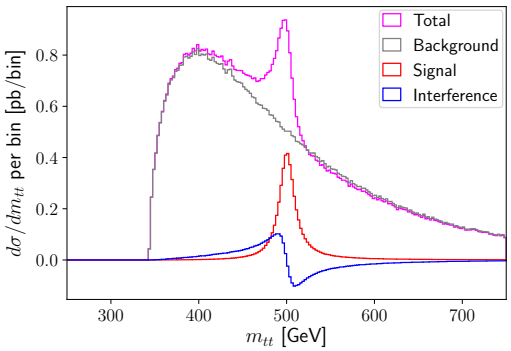

(b) $\mathrm{Br}(S \to \bar{t}t) = 0.06$, $\phi = 0$, $g_{tt} = 0.23$.

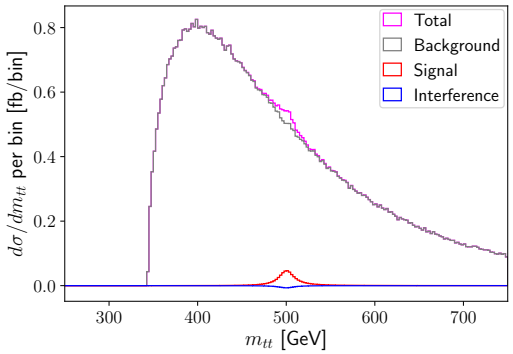

(c) $\mathrm{Br}(S \to \bar{t}t) = 0.0067$, $\phi = \frac{\pi}{2}$, $g_{tt} = 0.077$.

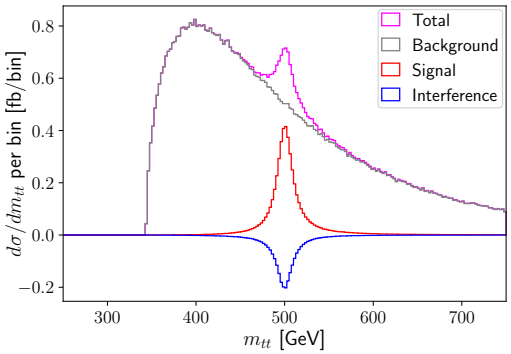

(d) $\mathrm{Br}(S \to \bar{t}t) = 0.06$, $\phi = \frac{\pi}{2}$, $g_{tt} = 0.23$.

Figure 19: Invariant mass distributions generated with MadGraph depending on g_{tt}. We show a singlet scenario with $\Gamma_s/m_s = 0.04$, $m_s = 500\,\mathrm{GeV}$ and $g_{gg} = 1.3 \times 10^{-3}\,\frac{1}{\mathrm{GeV}}$. The total distribution is shown in magenta, the background distribution in grey, the signal distribution in red and the interference distribution in blue. Bin size: 2.5 GeV

or the interference has a peak-dip shape whose sum vanishes, the partonic cross section of the signal $\hat{\sigma}_s$ and therefore the ratio S/B is proportional to g_{tt}^2. When the interference dominates the signal and has the shape of a Breit-Wiegner distribution, we expect that S/B is also proportional to g_{tt}, because the partonic cross section of the interference $\hat{\sigma}_i$ (Eq. (13)) is proportional to g_{tt}.

To verify this dependence numerically, we performed MadGraph simulations for $\phi = 0$ and $\phi = \frac{\pi}{2}$ using otherwise the default singlet scenario defined in Table 2 (with $\Gamma_s = 20\,\text{GeV}$, $g_{gg} = \frac{\alpha_s}{12\pi v}$, $m_s = 500\,\text{GeV}$) and coupling constants between $0.1 \leq g_{tt} \leq 0.73$, corresponding to branching ratios between a few percent and around 60%, computed using Eq. (35). We plot histograms showing the invariant mass distributions of the generated data and using these histograms then calculate and plot the ratio S/B as a function of g_{tt} (see Fig. 20).

In our chosen singlet scenario, the interference dominates the signal. Thus, for $\phi = \frac{\pi}{2}$, we can observe the relationship between g_{tt} and S/B that we expect from the partonic cross section of the interference Eq. (19) (see Fig. 20b). We can fit a straight line through the ratio S/B as a function of g_{tt} and obtain $S/B \approx -0.007 g_{tt}$. The S/B ratio is negative, because the interference is destructive (has a negative sign). However, for $\phi = 0$, the net effect of the interference on S/B is small, because the positive and negative events in the peak-dip distribution mostly cancel each other. Thus, we observe proportionality between g_{tt}^2 and S/B that we expect from the partonic cross section of the signal Eq. (13) (see Fig. 20a). We can fit a parabola through the ratio S/B as a function of g_{tt} and obtain $S/B \approx 0.0006 g_{tt}^2$. The fluctuations of the ratio S/B in Fig. 20a are caused by the statistical fluctuations of the interference. As the sum over the interference term vanishes apart from statistical fluctuations, the ratio S/B is smaller than for $\phi = \frac{\pi}{2}$ and thus, the importance of the statistical fluctuations compared to S/B increases. Fig. 20a is more zoomed in than Fig. 20b so the statistical fluctuations are better observable.

The obtained functions $S/B(g_{tt})$ only hold for the chosen singlet scenario, because A_i and A_s and therefore the S/B ratio as defined in Eq. (46) is influenced by all the other singlet parameters. For the chosen singlet scenarios the background is largely dominant and therefore the ratio S/B very small.

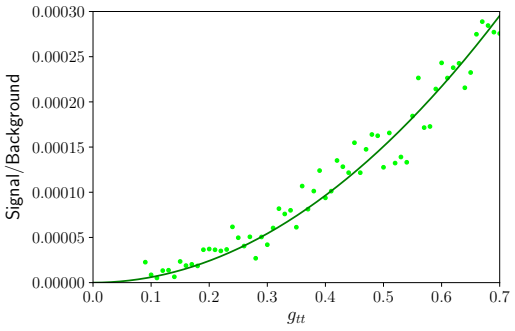

(a) $\phi = 0$. The straight line shows a parabola fitted on the data.

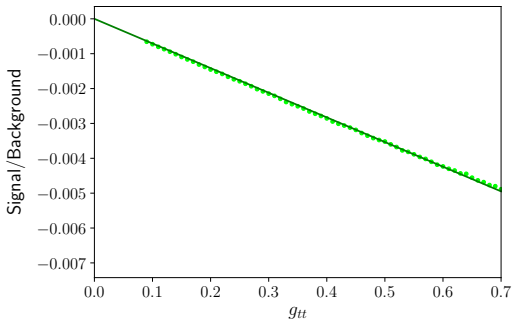

(b) $\phi = \frac{\pi}{2}$. The straight line shows a straight line fitted on the data.

Figure 20: Ratio S/B as a function of g_{tt} for a singlet scenario with $g_{gg} = \frac{\alpha_s}{12\pi v}$, $m_s = 500\,\text{GeV}$ and $\Gamma_s/m_s = 0.04$. The dots show the numerically determined S/B.

As the shape of the signal and interference are not influenced by g_{tt}, the detector resolution smears out the invariant mass distribution of singlet scenarios, that only differ by their g_{tt}, in the same way. Thus, we will not investigate the dependence of the smearing on g_{tt} further.

Height (difference) of the peak (and dip)

To quantify the dependence of the height (difference) of the peak (and dip) of the interference and signal, A_i and A_s, on g_{tt}, we compute A_i and A_s of the kinematic distributions for different values of g_{tt}. We use the same event samples as for plotting the ratio S/B as a function of g_{tt} and furthermore and computed the $\text{Br}(S \to t\bar{t})$ using Eq. (35). . We plot A_i and A_s not as a function

of g_{tt} but as a function of the physically more relevant parameter, S/B (see Fig. 21). For $\phi = 0$ we use the parabolic relationship between S/B and g_{tt} to convert g_{tt} into S/B and for $\phi = \frac{\pi}{2}$ we use the linear relationship between S/B and g_{tt} to convert g_{tt} into S/B. The partonic cross section of the interference (signal) term Eq. (19) (Eq. (13)) and its height (difference) of the peak (and dip) $\hat{A}_i$ ($\hat{A}_s$) is proportional to g_{tt} (g_{tt}^2) and thus for $\phi = 0$ proportional to $\sqrt{S/B}$ (S/B) and for $\phi = \frac{\pi}{2}$ proportional to S/B (S/B^2). This is in agreement with our numerical results shown in Fig. 21a.

The ratio of the interference to signal is proportional to $\frac{1}{g_{tt}}$ and therefore, proportional to $\frac{1}{\sqrt{S/B}}$ for $\phi = 0$ and to $\frac{1}{S/B}$ for $\phi = \frac{\pi}{2}$.

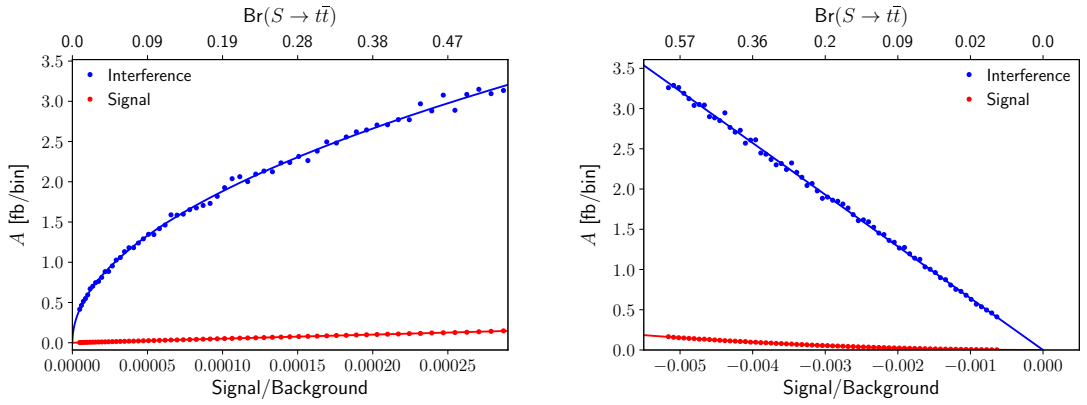

(a) $\phi = 0$.

(b) $\phi = \frac{\pi}{2}$

Figure 21: Height (difference) of the peak (and dip), A, of the signal distribution generated with MadGraph (red) and of the interference distribution (blue) depending on S/B. We show a singlet scenario with $g_{gg} = \frac{\alpha_s}{12\pi v}$, $\Gamma_s/m_s = 0.04$, $m_s = 500\,\text{GeV}$, $\phi = 0$ or $\phi = \frac{\pi}{2}$. In Fig. 21a, the red (blue) solid line shows straight (root function) fitted on the height (difference) of the peak (and dip) and in Fig. 21b, the red (blue) solid line show a parabola (line) fitted on the height (difference) of the peak (and dip). Bin size: 1.6 GeV.

Significance and total counting rate

Next, we want to determine the significance of the different distributions as a function of S/B using the same singlet scenarios and generated data for plotting S/B as a function of g_{tt} and A_i or A_s as a function of A/B. By definition, the significance of the signal including the interference is the ratio S/B multiplied by the constant factor $\sqrt{\sum_{m_{\text{tt,min}}}^{m_{\text{tt,max}}} \frac{\text{d}\sigma_B}{\text{d}m_{qq}}}$. This proportionality can be observed in Fig. 22. Furthermore, we observe that for the shown singlet scenarios, the significance of the signal and the interference at $\phi = 0$ are negligibly small, but the significance of the absolute value of the interference component can be above 5σ, if the g_{tt} and thus $|S/B|$ is large. Also for $\phi = \frac{\pi}{2}$ and large g_{tt}, the significance of the sum of interference and signal distribution is above 5σ. Thus, in that case the expected m_{tt} distribution contains no maximum, but a minimum under the continuum background. However, as discussed in Sect. 4.3, a higher significance obtained by choosing larger values of g_{tt} is limited by the requirement to choose Γ_s and g_{tt} consistently.

When calculating the total cross sections, we obtain similar dependences as when calculating the significances (see Table 3).

Summary

To conclude, we found that the interference is proportional to g_{tt} and the signal is proportional to g_{tt}^2. This was also observable when plotting the ratio signal to background, S/B, as a function of g_{tt}. Depending on the signal and background phase and on the relative size of the signal compared to the interference, the ratio S/B can be proportional to g_{tt}^2 (if the signal dominates the interference

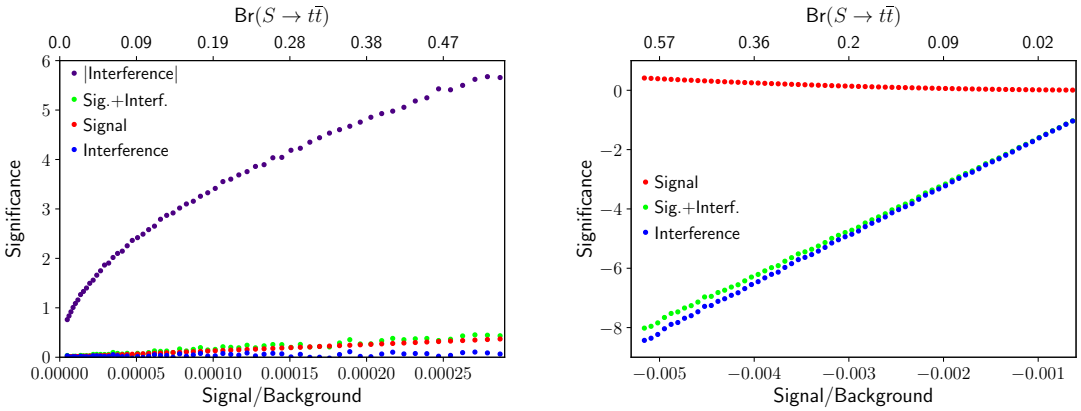

(a) $\phi = 0$.

(b) $\phi = \frac{\pi}{2}$.

Figure 22: Dependence of the significance over the QCD background on the ratio S/B. We show singlet scenarios with $\Gamma_s/m_s = 0.04$, $m_s = 500\,\text{GeV}$, $g_{gg} = \frac{\alpha_s}{12\pi v}$ and $\phi = 0$ or $\phi = \frac{\pi}{2}$. The significance of the interference is shown in blue, the significance of the signal alone in red, the significance of the signal including the interference in green and the purple dots in the left figure show the significance of the absolute values of the interference distribution.

Table 3: Total cross section of the interference and signal for different g_{tt} values. The total cross section of the background is $\sigma_{\text{B,tot}} = 453.26\,\text{pb}$

g_{tt}	$\sigma_{\text{s,tot}}$	$\sigma_{\text{i,tot}}$ for $\phi = 0$	$\sigma_{\text{i,tot}}$ for $\phi = \frac{\pi}{2}$
0.1	0.3461(70) pb	−8.265(88) pb	−50.02(6) pb
0.65	14.62(43) pb	−52.82(56) pb	−325.5(37) pb

and $\phi = \frac{\pi}{2}$), proportional to g_{tt} (if the interference dominates the signal and $\phi = 0$) or proportional to a sum of both (if signal and interference have the same size). We plotted the height (difference) of the peak (and dip), A_i and A_s, and the significances over the QCD background as a function of S/B and obtained the expected dependences.

In our chosen singlet scenario, the significance of the signal and of the interference for $\phi = 0$ are negligible. The significance of the absolute values of the interference and of the interference for $\phi = \frac{\pi}{2}$ are larger than 5σ for large g_{tt}.

5.6 Scalar-gluon coupling

In this section, we discuss the influence of the scalar-gluon coupling, g_{gg}, on the interference and the signal. In the previous sections, we chose a default singlet scenario with a scalar-gluon coupling of $g_{gg} = \frac{\alpha_s}{12\pi v}$, the value of the effective Higgs-gluon coupling. Higher values of g_{gg} are not typical for the simplest singlet models, but can easily be achieved in more complex extensions.

While varying g_{gg} and g_{tt}, we have to make sure that g_{gg}, g_{tt} and Γ_s are chosen consistently. For $g_{gg} = 0.001 \frac{1}{\text{GeV}}$, $g_{tt} = 0.73$ and $\Gamma_s = 20\,\text{GeV}$, the branching ratio for a decay of the scalar into gluons is $\text{Br}(S \to gg) = 0.29$ and for a decay into quarks $\text{Br}(S \to \bar{t}t) = 0.6$. We will generate data with Madgraph for singlet scenarios with $g_{tt} = 0.73$, $\Gamma_s = 20\,\text{GeV}$ and $g_{gg} \in [\frac{\alpha_s}{12\pi v}, 0.001 \frac{1}{\text{GeV}}]$ and calculate the height (difference) of the peak (and dip), A_i and A_s and the significance of the invariant mass distribution as a function of g_{gg}.

Height (difference) of the peak (and dip) and Significance as a function of g_{gg}

From our analytical calculations, we expect the same dependence of the signal and interference on g_{gg} as on g_{tt}: The partonic cross section of the signal Eq. (13) is proportional to g_{gg}^2 and the partonic cross section of the interference Eq. (19) is proportional to g_{gg}.

This is in agreement with the numerical results that we obtain when plotting A_i and A_s of the invariant mass distributions as a function of g_{gg} (see Fig. 23). The ratio of signal to interference increases with g_{gg} and therefore we can find regions where the signal is larger than the interference and the background. For example for a singlet scenario with $g_{gg} \approx 0.0009 \frac{1}{\text{GeV}}$, $\Gamma_s/m_s = 0.04$ and $\text{Br}(S \to \bar{t}t) = 0.6$, the signal is approximately 4.5 times larger than the interference. Thus, the interference is not as relevant any more. The branching ratio for the decay of the scalar into gluons is $\text{Br}(S \to gg) = 0.243$, when choosing $g_{gg} \approx 0.0009 \frac{1}{\text{GeV}}$. Choosing much larger values for g_{gg} than $g_{gg} \approx 0.0009 \frac{1}{\text{GeV}}$ would be unrealistic for the benchmark scenario with $\Gamma_s/m_s = 0.04$ and $\text{Br}(S \to \bar{t}t) = 0.6$, because that would lead to larger values of $\text{Br}(S \to gg)$ and thus the sum of $\text{Br}(S \to \bar{t}t)$ and $\text{Br}(S \to gg)$ would be larger than 1.

The dependence of the significance over the continuum background on g_{gg} for the different components (Fig. 23) is the same as the dependence of the significance on g_{tt} (Fig. 22). However, the significance we obtain are not just slightly above 5σ as observed when varying g_{tt}, but above 3000σ. In Sect. 5.5, when choosing $g_{gg} = \frac{\alpha_s}{12\pi v}$ and varying g_{tt} between 0.1 and 0.73, we cannot obtain much larger significances than 5σ because increasing g_{tt} much further than 0.73 would lead to values of $\text{Br}(S \to t\bar{t})$ above 1. As we can choose more than 100 times larger values for g_{gg} than the default value, without obtaining values of $\text{Br}(S \to gg)$ above one, it is possible to obtain a lot larger significances by varying g_{gg}.

In the scenario where the signal is approximately 4.5 times higher than the interference, the significance of the signal is over 7 times larger than the significance of the interference, and the signficance of the signal including the interference is above 3000σ. If a benchmark singlet scenario induces a signature of a significance of 3000σ at a luminosity of $300\,\text{fb}^{-1}$, it would most likely also already have been observed in LHC data with a lower luminosity.

However, there are singlet scenarios with larger g_{gg} than the effective Higgs-gluon coupling that are not yet excluded. If we choose, for example, $g_{gg} = 4\frac{\alpha_s}{12\pi v}$, the significance of the signal can be 5σ if we choose a sufficiently large value of g_{tt} and low value of Γ_s. Thus, in contrast to the scenarios in the previous section, a singlet scenario with $g_{gg} = 4\frac{\alpha_s}{12\pi v}$ would have a significance of above than 5σ even for $\phi = 0$ and can be relevant for LHC measurements.

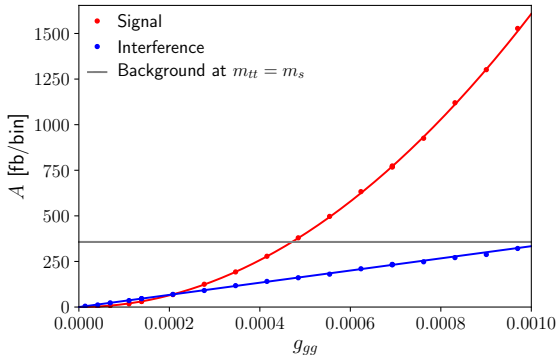

Figure 23: Height (difference) of the peak (and dip), A, of the signal distribution obtained with MadGraph (red dots) and the interference distribution (blue dots) depending on g_{gg}. We show singlet scenarios with $\Gamma_s/m_s = 0.04$, $g_{tt} = 0.73$, $\mathrm{Br}(S \to \bar{t}t) = 0.6$, $m_s = 500\,\mathrm{GeV}$ and $\phi = 0$. The red (blue) line shows parabola (line) fitted to the height (difference) of the peak (and dip). The solid grey line shows the background cross section of the histogram for the bin at $m_{tt} = m_s$. Bin size: 1.6 GeV.

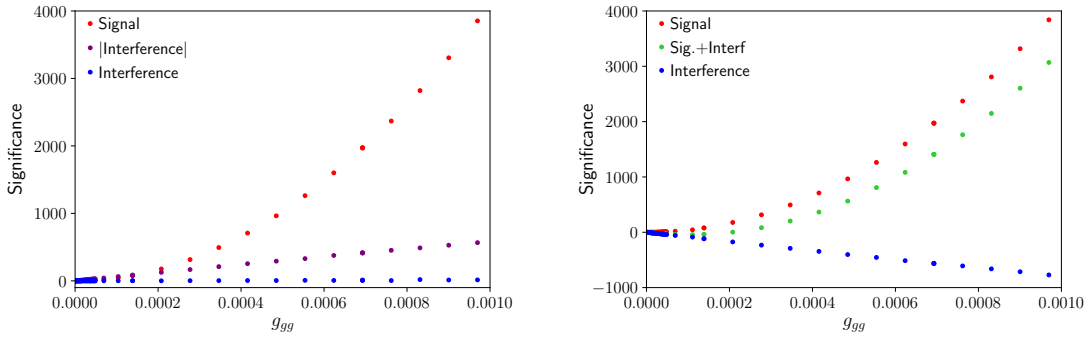

(a) $\phi = 0$. (b) $\phi = \frac{\pi}{2}$.

Figure 24: Significance over the continuum background of the different components as a function of g_{gg}. We generated data with MadGraph for singlet scenarios with $\Gamma_s/m_s = 0.04$, $m_s = 500\,\mathrm{GeV}$, $g_{tt} = 0.73$, $\mathrm{Br}(S \to \bar{t}t) = 0.6$ and $\phi = 0$. The significance of the interference is shown in blue, the significance of the signal in red, the significance of the signal including the interference in the right figure in green and the purple dots in the left figure show the significance of the absolute values of the interference distribution.

Singlet scenarios with a larger height of the signal peak than the height (difference) of the interference peak (and dip)

Even if the signal term has a significance of more than 5σ and the signal is larger than the interference, it is still necessary to consider the interference, because we need to take into account the shift in position and in size of the peak of the singal includin interference distribution due to the interference. Fig. 25 shows the position of the maximum of the signal including interference, $s_{\mathrm{max,i+s}}$, as a function of the phase, for a singlet scenario with with $\Gamma_s/m_s = 0.04$, $\mathrm{Br}(S \to \bar{t}t) = 0.6$ and $g_{gg} = 3.43 \times 10^{-4}\,\frac{1}{\mathrm{GeV}}$ (which is around 35 times higher than the effective coupling of the Higgs to gluons). In that case, the height of the signal peak, A_s, is 1.7 times higher than the height (difference) of the peak (and dip) of the interference A_i. Thus, the distribution of the signal including the interference has a peak, even for $\phi = \frac{\pi}{2}$. As expected, for $\phi = \frac{\pi}{2}$ and $\phi = \frac{3\pi}{2}$, where the interference is approximately Breit-Wiegner distributed, the position $s_{\mathrm{max,i+s}}$ is at the same position as the maximum of the signal. For $\phi = 0$ ($\phi = \pi$), the position $s_{\mathrm{max,i+s}}$ is shifted by the peak-dip-shape (dip-peak-shape) of the interference term to lower (higher) energies (see Fig. 25). The statistical fluctuations of the distribution and the binning effects are large. This could be overcome by producing samples with higher statistics.

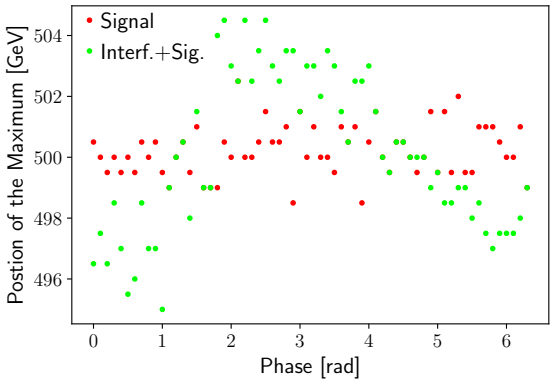

Figure 25: Position of the maximum of the signal distribution (red) and the signal including interference distribution (green) as a function of the phase, for a singlet scenario with $\Gamma_s/m_s = 0.04$, $\mathrm{Br}(S \to \bar{t}t) = 0.6$, $m_s = 500\,\mathrm{GeV}$, $g_{tt} = 0.73$, and $g_{gg} = 3.44 \times 10^{-4}\,1/\mathrm{GeV}$.

In the case where the influence of the interference on $s_{\mathrm{max,i+s}}$ is minimal, its influence on the height of the peak of the signal including interference A_{s+i} is maximal. This can be observed in Fig. 26, where we plot A_i, A_{s+i} and A_s as a function of the phase using the singlet scenarios described above. We find that for $\phi = 0$ and $\phi = \pi$, A_{s+i} is similar to A_s. For other phases, the Breit-Wiegner distributed part of the interference term shifts A_{s+i} to higher or lower values.

Summary

We found that the interference is proportional to g_{gg} and the signal is proportional to g_{gg}^2. When choosing values of g_{gg} that are considerably larger than the coupling between the SM Higgs and gluons, the signal is larger than the interference and can even be dominant compared to the background and the interference. However, very large values of g_{gg} induce significances of above 3000σ which would have likely already shown up in LHC data. For the case where the signal is larger than the interference, we plotted the dependence of of the position of its maximum and of the height (difference) of the peak (and dip) of the signal including the interference A_{s+i} on the phase. We found that, if the interference has the shape of a Breit-Wiegner distribution, A_{s+i} is lower (larger) than the height of the signal peak only, but the position of the maximum of the signal including the interference is at the same position as the maximum of the signal alone. When the interference has a peak-dip (dip-peak) shape, A_{s+i} does not differ that much from the height of the signal peak alone but the position of the maximum of signal including the interference is

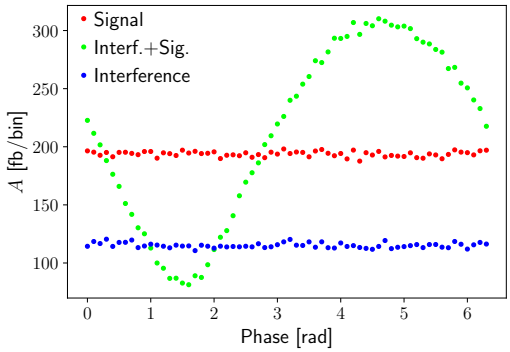

Figure 26: Height (difference) of the peak (and dip), A, of the distribution of the signal only (red), the interference only (blue) and the signal including the interference (green) as a function of the phase. We show results from MadGraph simulations with a singlet scenarios with $\Gamma_s/m_s = 0.04$, $\mathrm{Br}(S \to \bar{t}t) = 0.6$, $m_s = 500\,\mathrm{GeV}$, $g_{tt} = 0.73$, and $g_{gg} = 3.44 \times 10^{-4}\,\frac{1}{\mathrm{GeV}}$.

shifted to lower (higher) energies.

5.7 Constant branching ratio $\mathbf{Br}(S \to \bar{t}t)$

In Section 4.2.3 and 4.2.4 we have seen that the significance of the signal and the interference increase with g_{tt}, decrease with Γ_s and thus increases with $\mathrm{Br}(S \to \bar{t}t)$. The branching ratio $\mathrm{Br}(S \to \bar{t}t)$ given in Eq. (35) is proportional to $\frac{g_{tt}^2}{\Gamma_s}$. Having a value of $\mathrm{Br}(S \to \bar{t}t)$ below 100% assures that Γ_s and g_{tt} are chosen consistently. We want to investigate whether the significance is higher when Γ_s is low and g_{tt} large or the other way around for a given, fixed $\mathrm{Br}(S \to \bar{t}t)$.

From our previous numerical results (Section 4.2.3 and 4.2.4) and analytical calculations (Section 3.3.3) we know that the signal is proportional to $\frac{\Gamma_s^2}{g_{tt}^2}$ and the interference is proportional to $\frac{\Gamma_s}{g_{tt}}$. Thus, we expect when leaving the branching ratio and therefore $\frac{g_{tt}^2}{\Gamma_s}$ fixed, that A_s and A_i decrease with increasing Γ_s and decreasing g_{tt}.

This is in agreement with the results of our numerical simulations, where we fixed the branching ratio at 60% and varied the width between $\Gamma_s = 5\,\mathrm{GeV}$ and $\Gamma_s = 150\,\mathrm{GeV}$ and chose the coupling constant g_{tt} correspondingly as defined in Eq. (35) (i.e. $g_{tt} = (8\pi\Gamma_s \mathrm{Br}(S \to t\bar{t})/(\beta_q^3 3 m_s))^{0.5}$). Furthermore, we chose the default parameter $m_s = 500\,\mathrm{GeV}$ and $g_{gg} = \frac{\alpha_s}{12\pi v}$.

In Fig. 27 we show the significance of the invariant mass distributions over the continuum background of the different terms as a function of Γ_s/m_s. We observe that the significance is approximately constant from $\Gamma_s/m_s = 0.01$ until $\Gamma_s/m_s = 0.15$ and decreases for Γ_s/m_s larger than 0.15. The decrease is caused by the decrease of A_i. For the same reason, the significance of the signal decreases with Γ_s.

In total, we found that the significance of the signal and the interference does not change very much when leaving the branching ratio fixed but varying Γ_s and g_{tt}. The significance of the signal and the interference both decrease by less than 1σ when increasing Γ_s/m_s from 0.05 GeV to 0.3 GeV. We expect the same results when leaving the branching ratio $\mathrm{Br}(S \to gg)$ fixed and varying Γ_s and g_{gg}.

5.8 Quark mass and flavour

Until now, we have always discussed the process where the scalar decays into a pair of top quarks. The last remaining parameter is the quark mass m_q. Even though it is already measured to some accuracy, we will vary m_q to find how it influences the signal and the interference distribution. Furthermore, we will perform simulations with a pair of b quarks in the final state and compare them to our previous results.

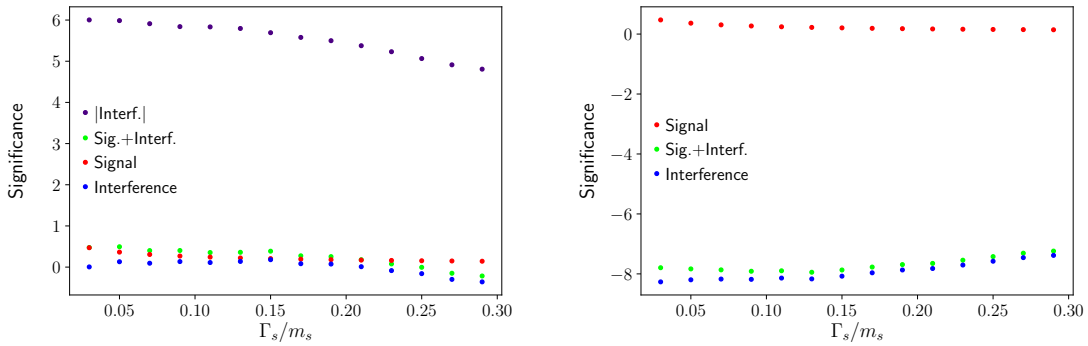

(a) $\phi = 0$. (b) $\phi = \frac{\pi}{2}$.

Figure 27: Dependence of the significance of different terms over the continuum background on Γ_s and g_{tt}. We choose a singlet scenario with $\mathrm{Br}(S \to \bar{t}t) = 0.6$, $m_s = 500\,\mathrm{GeV}$, $\phi = \frac{\pi}{2}$ and $g_{gg} = \frac{\alpha_s}{12\pi v}$. The significance of the interference is shown in blue, the significance of the signal only in red, the significance of the signal including the interference in green and the purple dots in the left Figure show the significance of the absolute values of the interference distribution.

Invariant mass distribution

In our analytical calculation in Sect. 3.2, we found that the partonic cross section of the signal Eq. (13) is proportional to the phase-space factor

$$\hat{\sigma}_s \propto \left(1 - \frac{(2m_q)^2}{\hat{s}}\right)^{\frac{3}{2}}, \tag{47}$$

and thus decreases with m_q. This can be explained by the fact that the higher the mass of the final state particles, the less phase space is available for the decay.

The partonic cross section of the interference given in Eq. (19) is

$$\hat{\sigma}_i \propto m_q \left[\operatorname{artanh}\left(\sqrt{1 - \frac{(2m_q)^2}{\hat{s}}}\right) - \sqrt{1 - \frac{(2m_q)^2}{\hat{s}}}\right]. \tag{48}$$

Thus, the cross section of the interference is zero for $m_q = 0$ ($\lim_{m_q \to 0} m_q \operatorname{artanh}\left(\sqrt{1 - (2m_q)^2/\hat{s}}\right) = 0$).

Fig. 28 shows the invariant mass distribution of a b-quark final state for a scalar singlet scenario with $\Gamma_s/m_s = 0.04$, $m_s = 500\,\mathrm{GeV}$, $g_{bb} = 0.23$, $\mathrm{Br}(S \to b\bar{b}) = 0.16$, and $g_{gg} = 1.3 \times 10^{-3}\,\frac{1}{\mathrm{GeV}}$ with and without background. We have chosen the same singlet parameters as in Fig. 19b including the same scalar-b-quark coupling as scalar-top-coupling. We observe that the background for a $b\bar{b}$ final state is significantly larger than for the $t\bar{t}$ final state. As expected from our analytical results, the differential cross section of the signal is larger but the differential cross section of the interference is significantly lower than when detecting a top quark final state. Thus, the ratio interference to signal is larger for the top decay.

Height (difference) of the peak (and dip)

We want to analyze the influence of m_q on the size of the interference and signal. From our analytical results in Sect. 3.3, we expect that the height of the signal peak $\hat{A}_s$ proportional to

$$\hat{A}_s \propto \left(1 - 1.5\frac{(2m_q)^2}{\hat{s}}\right). \tag{49}$$

The interference term given in Eq. (18) can be simplified by expanding a Taylor series around $m_{q,0} = 172\,\mathrm{GeV}$ and evaluating the Taylor series at $\hat{s} = m_s^2 = (500\,\mathrm{GeV})^2$, which gives us

$$\sigma_i \propto 158.17 - 0.458(m_q - 172) + 7.61 \times 10^{-3}(m_q - 172)^2 + O((m_q - 172)^3). \tag{50}$$

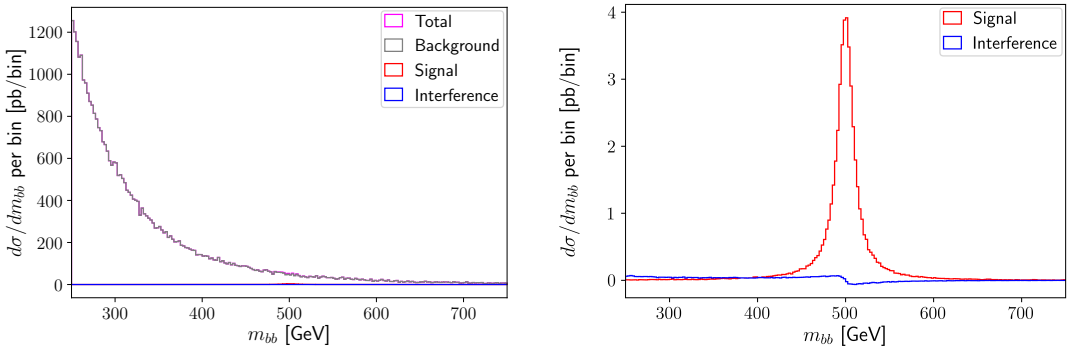

Figure 28: Invariant mass distributions for a b-quark final state generated with MadGraph. We show a singlet scenario with $\Gamma_s/m_s = 0.04$, $m_s = 500\,\text{GeV}$, $g_{bb} = 0.23$, $\text{Br}(S \to b\bar{b}) = 0.16$, and $g_{gg} = 1.3 \times 10^{-3}\,\frac{1}{\text{GeV}}$. The total distribution is shown in magenta, the background distribution in grey, the signal distribution in red and the interference distribution in blue. The right figure is a zoomed in version of the left figure.

Thus, we expect that the height (difference) of the interference peak (dip), $\hat{A}_i$, initially increases for low m_q, reaches a maximum and then decreases.

As for the mass of b-quarks, the Taylor series would not hold, we calculate $\hat{A}_s$ and $\hat{A}_i$ of the cross section Eq. (13) and Eq. (19) within the region $\hat{s} \in [250\,\text{GeV}, 750\,\text{GeV}]$ numerically for different values of m_q and plot the obtained $\hat{A}_s$ and $\hat{A}_i$ as a function of m_q (see Fig. 29). We observe similar behaviour as predicted by our calculation above.

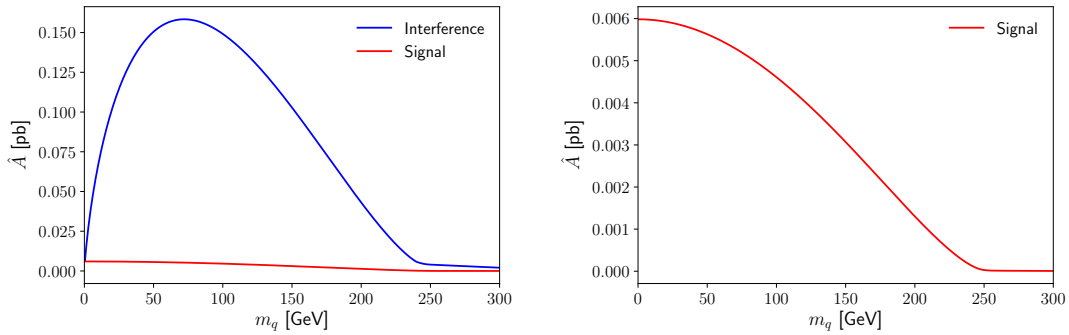

Figure 29: Height (difference) of the peak (and dip), $\hat{A}$, of the calculated partonic cross section of the signal (red line) and the interference (blue line) depending on m_q at $g_{qq} = 0.4485$, $g_{gg} = \frac{\alpha_s}{12\pi v}$, $\phi = \frac{\pi}{2}$, $m_s = 500\,\text{GeV}$ and $\Gamma_s/m_s = 0.04$. The right Figure is a zoomed in version of the left figure. Bin size: 2.5 GeV.

We obtain numerical results with MadGraph by generating $gg \to t\bar{t}$ or $gg \to b\bar{b}$, with various values of the top/bottom mass. The results we obtain when generating $gg \to t\bar{t}$ for different top masses are the same up to statistical fluctuations, as for $gg \to b\bar{b}$ when choosing the same masses. Thus, we will only show the results obtained by generating $gg \to t\bar{t}$ for top quark masses $m_q \in [4.7\,\text{GeV}, 172\,\text{GeV}]$ for a singlet scenario with $g_{qq} = 0.4485$ and otherwise default parameter ($m_s = 500\,\text{GeV}$, $g_{gg} = \frac{\alpha_s}{12\pi v}$, $\phi = \frac{\pi}{2}$, $\Gamma_s/m_s = 0.04$) and corresponding $\text{Br}(S \to t\bar{t})$ computed using Eq. (35). We set the minimum invariant mass of the pair of quarks to 250 GeV to avoid that the total cross section is dominated by the differential cross section of the bb-background at low energies just above the bb-threshold. Fig. 30 shows the height (difference) of the peak (and dip), A_i and A_s, obtained from the generated invariant mass distributions as a function of m_q. The numerical results we obtained with MadGraph are in good agreement with our analytical

predictions shown in Fig. 29. We observe that the A_s decrease with increasing m_q because of the reduction in available phasespace for the decay. The maximum of A_i is at approximately $m_q \approx 95\,\text{GeV}$. For $2m_q > m_s$, the scalar has to be produced off-shell, which is possible because of the Heisenberg uncertainty principle. As we chose $\Gamma_s = 20\,\text{GeV}$, we can still observe events when the mass of the quark pair is slightly larger than m_s. However, when increasing the quark mass further, the cross section of the signal and the interference approach zero (see Fig. 30).

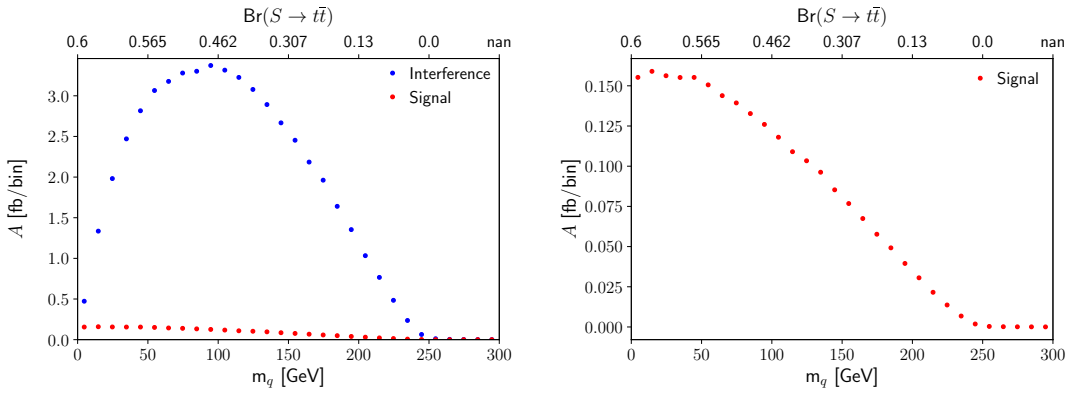

Figure 30: Height (difference) of the peak (and dip), A, of the invariant mass distributions generated with MadGraph of the signal (red dots) and the interference (blue dots) depending on m_q at $g_{qq} = 0.4485$, $g_{gg} = \frac{\alpha_s}{12\pi v}$, $\phi = \frac{\pi}{2}$, $m_s = 500\,\text{GeV}$ and $\Gamma_s/m_s = 0.04$. The right figure is a zoomed in version of the left figure. Bin size: 1.6 GeV.

Significance

Next, we want to observe the influence of the quark mass on the significance. The total cross section of the background and therefore its statistical error decreases with the increasing quark mass, due to the reduction of the available phase space for the decay. Because of the lowered statistical error of the background, the significance of the signal over the background increases until $m_q \approx 100\,\text{GeV}$ even though the signal cross section decreases (see Fig. 31). However, for larger quark masses, the effect of the decrease of the signal cross section becomes more relevant and therefore the significance of the signal decreases. Similar to A_i, the significance of the interference also reaches a maximum and then decrease (see Fig. 31). The maximum of the significance is at $m_q \approx 140\,\text{GeV}$ and thus around 40 GeV shifted to larger quark masses compared to the maximum of A_i. This can be explained by the decrease of the size of the background with the quark mass.

In total, the significances of the signal and of the interference for a given Γ_s and g_{qq} are higher for a decay into top quarks, than for a decay into b-quarks. Also, the branching ratio decreases with m_t, so we can choose higher values of g_{tt}, than of g_{bb} for a given width and branching ratio. Thus, we expect lower significances if we observe the decay of the scalar into lighter quarks.

Simulation with a b-pair in the final state

We have investigated the dependence of A_s and A_i and of the significances on m_q for a benchmark singlet scenario. Next, we want to analyze the process where the scalar decays into a pair of b-quarks for different singlet scenarios. From our observations above, we expect that for a given singlet scenario, the significance of the interference and the height (difference) of its peak (and dip), A_i, is lower when detecting b quarks in the final state instead of t-quarks. However, the general dependence of the invariant mass distributions and their heights on the different parameters should be the same.

This is in agreement with the results that we obtain when generating event samples of $gg \to bb$ with Madgraph. We have varied the scalar-b-quark coupling, using the same singlet scenario as the one where we varied the scalar-top-coupling in Sect 5.5 ($m_s = 500\,\text{GeV}$, $g_{gg} = \frac{\alpha_s}{12\pi v}$ and

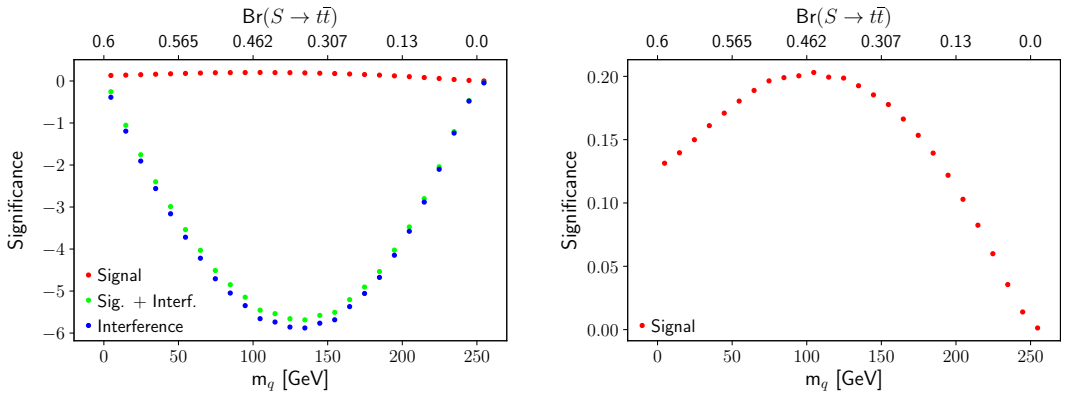

Figure 31: Dependence of the significance of the different components over the continuum background on m_q. We choose a singlet scenario with $g_{gg} = \frac{\alpha_s}{12\pi v}$, $m_s = 500\,\text{GeV}$, $\phi = \frac{\pi}{2}$ and $\Gamma_s/m_s = 0.04$. The significance of the interference is shown in blue, the significance of the signal in red and the significance of the signal including the interference in green. The right figure is a zoomed in version of the left figure.

$\text{Br}(S \to \bar{b}b) < 0.6$). From thar, we calculated the S/B ratio as defined in Eq. (46) and found that for $\phi = 0$, when the interference does not contribute significantly to the S/B ratio, the ratio of S/B is around 9 times lower when detecting b-quarks instead of top quarks ($S/B = g_{bb}^2 \cdot 6.86 \times 10^{-5}$). This can be explained by the fact the background of $b\bar{b}$ final states is larger. For $\phi = \frac{\pi}{2}$, the ratio S/B is 64 times lower than for a decay into top quarks ($S/B = -11 \times 10^{-5} g_{bb}$). As explained above, this is because the interference, which in the chosen benchmark scenario is dominant compared to the signal, is suppressed by the quark mass (see Eq. (19)).

In Appendix B, Fig. 33 , Fig. 34 , Fig. 35 we show the significance over the continuum background as a function of ϕ, Γ_s and g_{bb} for singlet scenarios using the default parameter defined in Table 2 for the other parameters ($g_{gg} = \frac{\alpha_s}{12\pi v}$, $m_s = 500\,\text{GeV}$). We observe a similar dependence of the significances on the different parameters as for the top-quark final state but with distinctly lower significances below 5σ. The ratio of the signal significance and of A_s to the interference significance and A_i is larger for a decay of the scalar into b quarks than for a decay into top quarks (see Fig. 30). However, if we choose default parameters ($m_s = 500\,\text{GeV}$, $g_{gg} = \frac{\alpha_s}{12\pi v}$ and $\text{Br}(S \to \bar{b}b) < 0.6$), A_s is at a maximum of 20% of A_i. If we increase m_s, the ratio of signal to interference increases. At $m_s = 2\,\text{TeV}$, $\Gamma_s = 400\,\text{GeV}$, $g_{gg} = 2\frac{\alpha_s}{12\pi v}$ and $\text{Br}(S \to \bar{b}b) = 0.6$, A_s and A_i have the same size. However, in that case, the significance of the signal including the interference is only approximately 0.01σ.

If we choose a singlet scenario with $\text{Br}(S \to b\overline{b}) = 0.6$, $\Gamma_s = 20\,\text{GeV}$ and $m_s = 500\,\text{GeV}$, the significance of the signal including the interference is above 5σ for $g_{gg} \geq 0.000\,056\,\frac{1}{\text{GeV}}$ if $\phi = 0$ and for $g_{gg} \geq 0.000\,09\,\frac{1}{\text{GeV}}$ if $\phi = \frac{\pi}{2}$ (see Appendix Fig. 36). As, in this parameter range even for $\phi = \frac{\pi}{2}$, the contribution of the signal to the total counting rate is larger than the contribution of the interference, we will not observe with a significance of above 5σ a dip in the total counting rate. This would only be possible when increasing the luminosity or the detection efficiency.

Summary

In this section we observed that the height (difference) of the peak (and dip) of the interference invariant mass distribution, A_i, is considerably larger when we detect a pair of top quarks in the final state, than when we detect other types of quarks. In contrast, the height of the peak of the signal invariant mass distribution, A_s, is larger for a decay into lighter quarks than for a decay into top quarks. However, as also the cross section of the background and thus its statistical error decreases with increasing quark mass, the significance over the continuum background of signal, interference and signal including interference is distinctly larger, when detecting top quarks than

when detecting lighter types of quarks. In our benchmark case, the significance of the signal including the interference of a decay into b-quarks is only for singlet scenarios with $g_{gg} > 0.000\,08\,\frac{1}{\text{GeV}}$ above 5σ. In these scenarios the contribution of the signal to the scalar signature is larger than the contribution of the interference, so that, for the chosen luminosity and detection efficiencies and even if $\phi = \frac{\pi}{2}$, we do not observe a dip below the continuum background. If we observed the decay into even lighter quarks than b-quarks, we would obtain even lower significances. This motivates our initial choice to use the decay channel into top quarks to investigate the dependence of the interference on the singlet parameters.

6 Conclusion

In this thesis, we have systematically studied the interference effect in the production of a new scalar particle during pp-collisions, which decays into a pair of quarks. We have calculated the partonic cross section of the signal, interference and background analytically and generated, for various different scalar singlet scenarios, the hadronic differential cross sections of the different components using MadGraph. This allowed us to determine the dependence of the differential cross sections and their sizes on the different parameters related to the scalar.

We found that the mass of the scalar and its width are the most important parameters for the position and widening of the peak/dip of the invariant mass distribution for the interference and the signal. Furthermore, the line-shape of the interference distribution strongly depends on the difference of the complex phases of the signal and the background transition amplitudes: In the case of $\phi = 0$ or $\phi = \pi$, the interference has an anti-symmetric bump-dip or dip-bump structure around the resonance mass. In that case, the net effect of the interference on the total cross section of the signal including the interference is small. However, the interference can shift the peak of the differential cross section of the signal including the interference to lower/higher energies. For a phase difference of $\phi = \frac{\pi}{2}$ or $\phi = \frac{3\pi}{2}$, the interference has a Breit-Wigner-shaped bump or dip at the resonance mass. In that case the interference does not influence the position of the mass peak but contributes to the total cross section.

To quantify the size of the interference and the signal and compare their sizes both to each other and to the background, we calculated the height (difference) of the peak (and dip) of their differential cross sections as a function of the different parameters. We found that the height of the signal peak, A_s, increases as $\frac{g_{qq}^2 g_{gg}^2}{\Gamma_s^2}$ and of the height (difference) of the peak (and dip) of the interference, A_i, increases as $\frac{g_{qq} g_{gg}}{\Gamma_s}$. Thus, the smaller g_{gg}, g_{qq} and the larger Γ_s, the larger the ratio of the height of the interference term, A_i to the height of the signal peak A_s and thus the larger the relative contribution of the interference to the scalar signature. Furthermore, we found that A_s and A_i do not depend on the signal and background phases. Moreover, A_i decreases with the scalar mass and A_s reaches a maximum (in our benchmark scenario at $m_s = 600\,\text{GeV}$) and decreases afterwards. The ratio of A_i to A_s decreases with m_s.

Using the described dependences, we found singlet scenarios where the interference term dominates the signal component. If we choose, for example, a top quark final state, $\Gamma_s = 20\,\text{GeV}$, $m_s = 500\,\text{GeV}$, $\text{Br}(S \to \bar{t}t) \leq 0.6$ and $g_{gg} < 0.0002\,\frac{1}{\text{GeV}}$, A_i is larger than A_s. For singlet scenarios with $g_{gg} = g_{ggH} = \frac{\alpha_s}{12\pi v}$, we found that A_i is considerably larger than A_s for all examined singlet scenarios that are listed in Table 2. Thus, for these singlet scenarios and if $\phi = \frac{\pi}{2}$, the invariant mass distribution of the signal including the interference includes a dip rather than the well-known Breit-Wigner peak.

To answer the question whether the signatures of the scalar singlet are relevant for LHC measurements, we calculated the significance of the different components over the continuum background on parton level. We found that, similar to the height (difference) of the peak (and dip), the significance of interference and signal increase with g_{tt}/Γ_s. We can find scenarios where the signature of the scalar singlet is only relevant due to the interference contribution. For example, for $m_s = 500\,\text{GeV}$, $g_{gg} = \frac{\alpha_s}{12\pi v}$, $\text{Br}(S \to \bar{t}t) \leq 0.6$ and $\phi = 0$, the significance of the signal including the interference is below 5σ, because the sum over the peak-dip shaped interference vanishes. However, using the same parameters but $\phi = \frac{\pi}{2}$, where the interference has the shape of a dip, the significance of the signal including the interference is larger than 5σ if $\text{Br}(S \to \bar{t}t) = 0.6$. Even

for branching ratios slightly smaller than 60% we got a significance above 5σ if we choose Γ_s/m_s between around 0.14 to 0.2. For these scenarios an analyzing method of experimental data that includes the interference contribution and searches for a dip in the total counting rate instead of the usual excess is necessary to discover the scalar. Concerning the dependence of the significance on m_s, we found that the significance of the signal increases with m_s. For our benchmark scenario, the significance of the interference and of signal including the interference increase slightly until m_s is around 550 GeV, but decreases after this point. In total, we obtain larger significance of the signal and the interference terms by choosing a larger value for the scalar-gluon coupling g_{gg} than the default value of $g_{gg} = \frac{\alpha_s}{12\pi v}$.

When detecting a pair of lighter quarks than top-quarks in the final state, we obtain considerably smaller heights (differences) of the peaks (and dips) of the interference, A_i, but larger heights of the signal peak, A_s and thus larger values for the ratio signal to interference. However, the signal to background ratio and thus also the significance of the signal and of the interference over the background is distinctly lower than for the top-pair final state. For our benchmark singlet scenarios where we chose a large enough value of g_{gg}, so that the significance of the signal including the interference is larger than 5σ, A_s was larger than A_i.

A list of the maximum and minimum significances of the interference over the continuum background, that we found when varying the different scalar parameters within the ranges defined in Table 2 can be found in Appendix C in Tab. 4.

When taking detector resolution effects into account, we observe that the invariant mass distribution gets wider with lower A_i and A_s and lower significance. This is more pronounced for small width and for a peak-dip shaped interference term instead of the Breit-Wiegner shaped one.

We were able to predict the dependence of the shape, height (difference) of the peak (and dip) and significance of the signal, interference and signal including interference on different parameters. The next step for this study is to include parton showers, detector simulations and more background events e.g. fake tops (a pair of b-quarks that has been misidentified as top pair). This would allow to compare our results to experimental findings. Furthermore, one could take into account the possibility of QCD radiation in the final state. Hespel et. al. found that the relative size of the interference does not change when taking QCD radiation into account by including an extra jet in the final state [10]. Our results could also be influenced by NLO contributions. Including the NLO leads to large QCD corrections of the signal [10]. The ratio signal to background and interference to background is larger when including NLO corrections [10].

The decay of the scalar into top quarks is not the only decay channel that could possibly be observed at the LHC. Another possible decay mode of the scalar would be a decay into a lepton pair. In general, we expect to obtain similar results as for the decay into a quark pair but with considerably lower cross sections of the signal and interference. This is because the lepton masses are a lot smaller than the top quark mass and thus the coupling to the scalar particle is lower. Furthermore, we have observed that the interference term decreases to zero in the limit of negligible fermion masses.

The scalar could also decay into pair of Higgs bosons. However, in that case, we would obtain almost no interference contribution because the background, meaning the SM rate of a Higgs pair production, is very low [10].

Another interesting channel would be the decay of the scalar into vector bosons. Vector bosons have a fundamentally different structure than the fermions. Thus, it is not possible to apply predictions based on the study of the interference of the scalar with the QCD background to the interference between the scalar and vector bosons. An example that has been studied in literature is the interference between a scalar decaying into $\gamma\gamma$ and the loop-induced background [8]. It has been shown that the line-shape of the interference distribution for a $\gamma\gamma$ final state is similar to the one of the interference term with the QCD background [8]. Especially if the signal cross section is small compared to the background, the $\gamma\gamma$-interference can have a significant influence on the shape of the invariant mass distribution and on the total counting rate [8]. However, the interference effects have a smaller impact than in the case of a top-pair final state [8].

Various BSM models not only predict new scalar particles but also other new particles that could be produced at hadron colliders and whose amplitudes could interfere with SM processes. If we consider, for example, the production of a pseudoscalar, the interference effects should be compa-

rable to the interference between the scalar singlet and the QCD background. Hespel et. al. found that the invariant mass distribution of the interference of a pseudoscalar with the $t\bar{t}$ background indeed approximately resembles in line-shape and dependence on Γ_s to the one of a scalar [10]. The total cross section of the signal and interference of the pseudoscalar is a bit larger than the one of the scalar when using the same resonance masses and width [10]. For the interference effects in the production of new heavy fermions or new vector bosons predicted by BSM scenarios, the structure of the signal and background is completely different to the one of the production of a scalar. Thus, predictions of the interference terms would require new analyses.

To conclude, we found that interference effects in the production of a BSM scalar singlet particle decaying into a pair of top quarks can influence the total cross section and the shape of the key signature of the scalar resonance. We found scenarios where the interference dominates and induced, for example, a dip below the continuum background. Thus, to obtain precise results, inference effects should be taken into account when analyzing experimental data.

Acknowledgements

First of all, I would like to thank Johann Brehmer for the helpful discussions and for always taking time and patience to answer my questions! Furthermore, I would like to thank Tilman Plehn for giving me this great opportunity to get an insight into actual research and being always available for discussions and to answer questions. A special thanks also goes to Jennifer Thompson and Susanne Westhoff for proof-reading this thesis. Finally, I would like to give my thanks to the entire research group for the openness and kindness!

References

[1] J. Alwall *et al.*, 'The automated computation of tree-level and next-to-leading order differential cross sections, and their matching to parton shower simulations,' JHEP **1407**, 079 (2014) doi:10.1007/JHEP07(2014)079 [arXiv:1405.0301 [hep-ph]].

[2] The Atlas collaboration, 'ATLAS Exotics Searches-p5% CL Upper Exclusion Limits', July 2017, `https://atlas.web.cern.ch/Atlas/GROUPS/PHYSICS/CombinedSummaryPlots/EXOTICS/ATLAS_Exotics_Summary/ATLAS_Exotics_Summary.png`

[3] CMS Exotica Physics Group Summary, 'Summary of results on exotic physics, Resonances, extra dimensions', ICHEP 2016, `https://twiki.cern.ch/twiki/pub/CMSPublic/PhysicsResultsCombined/exo-limits_ICHEP_2016.pdf`

[4] CERN 2017, 'The Large Hadron Collider', 28. Aug. 2017, `http://home.cern/topics/large-hadron-collider`

[5] The ATLAS collaboration [ATLAS Collaboration], 'Search for heavy Higgs bosons A/H decaying to a top-quark pair in pp collisions at $\sqrt{s} = 8$ TeV with the ATLAS detector,' ATLAS-CONF-2016-073.

[6] S. P. Martin, 'Shift in the LHC Higgs diphoton mass peak from interference with background,' Phys. Rev. D **86**, 073016 (2012) doi:10.1103/PhysRevD.86.073016 [arXiv:1208.1533 [hep-ph]].

[7] J. Campbell, M. Carena, R. Harnik and Z. Liu, 'Interference in the $gg \to h \to \gamma\gamma$ On-Shell Rate and the Higgs Boson Total Width,' arXiv:1704.08259 [hep-ph].

[8] A. Djouadi, J. Ellis and J. Quevillon, 'Interference effects in the decays of spin-zero resonances into $\gamma\gamma$ and $t\bar{t}$,' JHEP **1607**, 105 (2016) doi:10.1007/JHEP07(2016)105 [arXiv:1605.00542 [hep-ph]].

[9] M. Carena and Z. Liu, 'Challenges and opportunities for heavy scalar searches in the $t\bar{t}$ channel at the LHC,' JHEP **1611**, 159 (2016) doi:10.1007/JHEP11(2016)159 [arXiv:1608.07282 [hep-ph]].

[10] B. Hespel, F. Maltoni and E. Vryonidou, 'Signal background interference effects in heavy scalar production and decay to a top-anti-top pair,' JHEP **1610**, 016 (2016) doi:10.1007/JHEP10(2016)016 [arXiv:1606.04149 [hep-ph]].

[11] Wikipedia, 'Standard Model', `https://en.wikipedia.org/wiki/Standard_Model`, 25. Aug. 2017

[12] Povh B, Rith K, Scholz C, Zetsche F, Rodejohann W. 'Teilchen und Kerne: Eine Einführung in die physikalischen Konzepte'. 9th ed. Berlin, Heidelberg: Springer Spektrum; 2014. doi:10.1007/978-3-642-37822-5.

[13] Peskin ME, Schroeder DV. 'An Introduction to Quantum Field Theory'. [Boulder]: Westview Press, a member of the Perseus Books Group; 2016.

[14] G. Aad *et al.* [ATLAS Collaboration], 'Observation of a new particle in the search for the Standard Model Higgs boson with the ATLAS detector at the LHC,' Phys. Lett. B **716**, 1 (2012) doi:10.1016/j.physletb.2012.08.020 [arXiv:1207.7214 [hep-ex]].

[15] B. Patt and F. Wilczek, 'Higgs-field portal into hidden sectors,' hep-ph/0605188.

[16] C. Englert, T. Plehn, D. Zerwas and P. M. Zerwas, 'Exploring the Higgs portal,' Phys. Lett. B **703**, 298 (2011) doi:10.1016/j.physletb.2011.08.002 [arXiv:1106.3097 [hep-ph]].

[17] T. Robens and T. Stefaniak, 'Status of the Higgs Singlet Extension of the Standard Model after LHC Run 1,' Eur. Phys. J. C **75**, 104 (2015) doi:10.1140/epjc/s10052-015-3323-y [arXiv:1501.02234 [hep-ph]].

[18] D. López-Val and T. Robens, 'ΔR and the W-boson mass in the singlet extension of the standard model,' Phys. Rev. D **90**, 114018 (2014) doi:10.1103/PhysRevD.90.114018 [arXiv:1406.1043 [hep-ph]].

[19] CERN, Education, Communications and Outreach Group, 'LHC the guide', February 2017 CERN-Brochure-2017-002-Eng, 29.08.2017, `http://cds.cern.ch/record/2255762/files/CERN-Brochure-2017-002-Eng.pdf`

[20] T. Plehn, 'Lectures on LHC Physics,' Lect. Notes Phys. **886** (2015). doi:10.1007/978-3-319-05942-6

[21] T. Han, 'Collider phenomenology: Basic knowledge and techniques,' *doi* : 10.1142/9789812773579_0008 hep-ph/0508097.

[22] CERN 2017 ,'The High-Luminosity LHC', 29. Aug. 2017, `http://home.cern/topics/high-luminosity-lhc`

[23] Schwartz MD. 'Quantum Field Theory and the Standard Model'. Cambridge [u.a.]: Cambridge University Press; 2014.

[24] Burgess CP, Moore GD. 'The Standard Model: A Primer'. 1st ed. Cambridge [u.a.]: Cambridge Univ. Press; 2013.

[25] J. Alwallet.al. 'MadEvent a multi-purpose event generator powered by MadGraph Minimal User Guide', 01th March 2007, `https://cp3.irmp.ucl.ac.be/projects/madgraph/wiki/ManualAndHelp`

[26] C. Patrignani et al. (Particle Data Group), Chin. Phys. C, 40, 100001 (2016).

[27] M. Aaboud *et al.* [ATLAS Collaboration], 'Measurements of top-quark pair differential cross-sections in the lepton+jets channel in pp collisions at $\sqrt{s}$=13 TeV using the ATLAS detector,' arXiv:1708.00727 [hep-ex].

[28] ATLAS Collaboration, 'Boosted hadronic top identification at ATLAS for early 13 TeV data', ATL- PHYS-PUB-2015-053, 2015, `https://cdsweb.cern.ch/record/2116351`.

[29] G. Aad *et al.* [ATLAS Collaboration], 'A search for $t\bar{t}$ resonances using lepton-plus-jets events in proton-proton collisions at $\sqrt{s} = 8$ TeV with the ATLAS detector,' JHEP **1508**, 148 (2015) doi:10.1007/JHEP08(2015)148 [arXiv:1505.07018 [hep-ex]].

[30] Brock I, ed. Physics at the Terascale. 1st ed. Weinheim: Wiley-VCH; 2011.

Appendices

A. Feynman rules of the Scalar S

The Feynman rules for coupling of the scalar to SM particles are shown in Fig. 32.

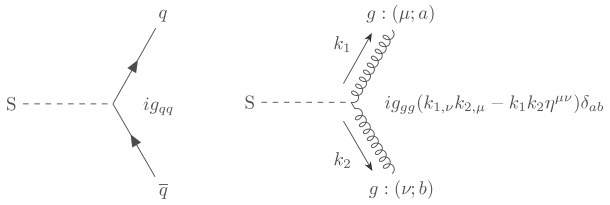

(a) Coupling scalar S to quarks.

(b) Coupling scalar S to gluons.

Figure 32: Feynman rules for vertices between two fermions and the Scalar S (left Figure) and the Scalar S and two gluons (right Figure).

B. Simulations with a pair of b-quarks in the final state

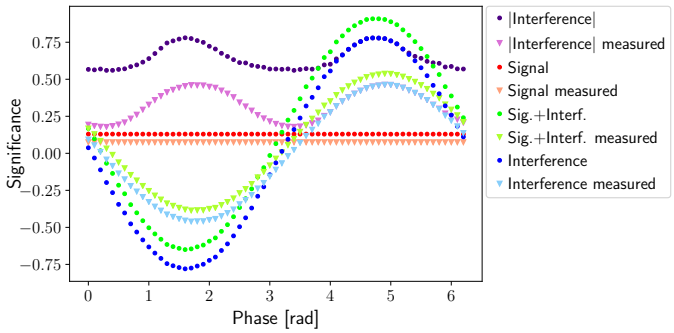

Figure 33: Dependence of the significance over the QCD background on ϕ. We show a singlet scenario with $\Gamma_s/m_s = 0.04$, $g_{gg} = \frac{\alpha_s}{12\pi v}$, $g_{bb} = 0.41$, $\mathrm{Br}(S \to b\bar{b}) = 0.5$, $m_s = 500\,\mathrm{GeV}$ and detect a pair of b-quarks in the final state. The significance of the interference is shown in blue, the significance of the signal in red, the significance of the signal including the interference in green and the significance of the absolute value of the interference distribution in purple. The darker coloured dots show the significance of the generated distributions, the lighter coloured dots show the significance of the distributions including resolution effects.

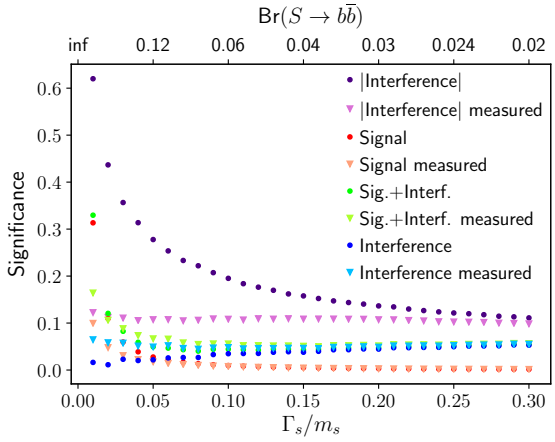

Figure 34: Dependence of the significance over the QCD background on Γ_s/m_s. We show a singlet scenario with $g_{bb} = 0.22$, $g_{gg} = \frac{\alpha_s}{12\pi v}$, $m_s = 500\,\text{GeV}$ and detect a b-quarks final state. The significance of the interference is shown in blue, the significance of the signal in red and the significance of the signal including the interference in green and the purple dots show the significance of the absolute value of the interference distribution. The darker coloured dots show the significance of the generated distributions, the lighter coloured dots show the significance of the distributions including resolution effects.

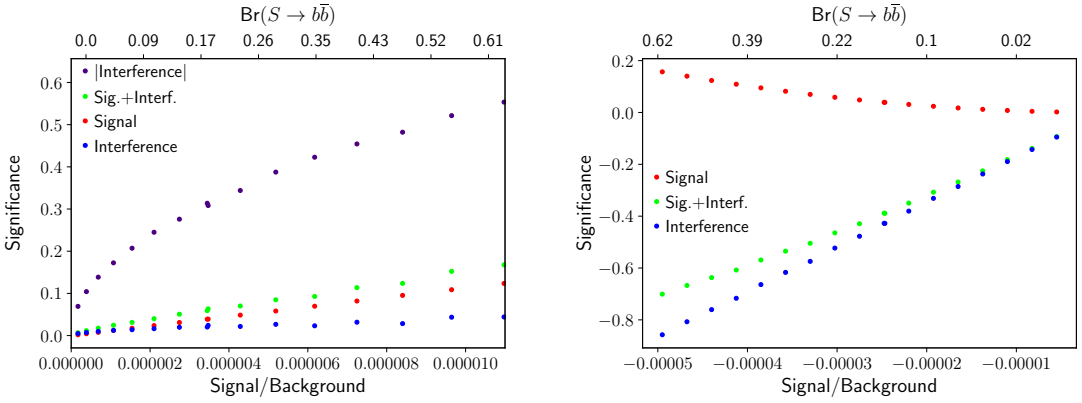

(a) $\phi = 0$. (b) $\phi = \frac{\pi}{2}$.

Figure 35: Dependence of the significance over the QCD background on the ratio S/B. We show a singlet scenario with $\Gamma_s/m_s = 0.04$, $g_{gg} = \frac{\alpha_s}{12\pi v}$, $m_s = 500\,\text{GeV}$ and detect a b-quarks final state. The significance of the interference is shown in blue, the significance of the signal in red and the significance of the signal including the interference in green and the purple dots in the left figure show the significance of the absolute value of the interference distribution.

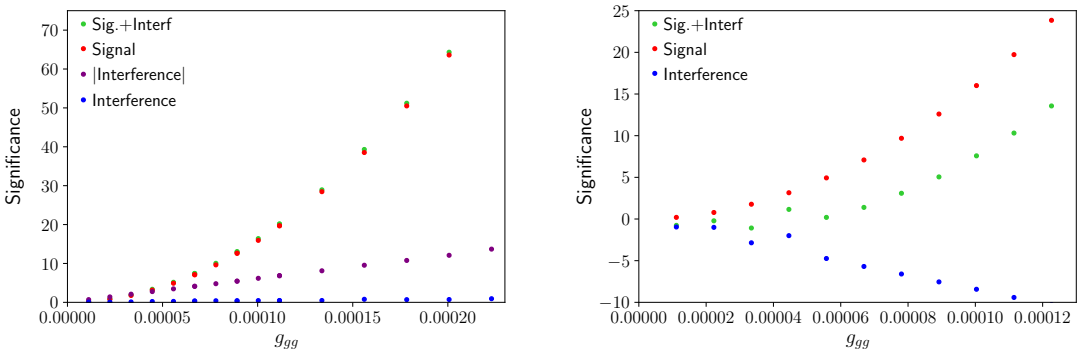

(a) $\phi = 0$. (b) $\phi = \frac{\pi}{2}$.

Figure 36: Significance over the continuum background of the different components as a function of g_{gg}. We generated data with MadGraph for singlet scenarios with $\Gamma_s/m_s = 0.04$, $m_s = 500\,\text{GeV}$, $\text{Br}(S \to \bar{b}b) = 0.6$ and $\phi = 0$. The significance of the interference is shown in blue, the significance of the signal in red, the significance of the signal including the interference in green and the purple dots in the left figure show the significance of the absolute values of the interference distribution.

C. Overview over Significances

Table 4: Maximum and minimum significance of the interference over the continuum background when varying the parameter x; $x_{\min}$ ($x_{\max}$) is the value of the investigated parameter, where the significance of the interference reaches its maximum (minimum) within the investigated parameter range, denoted as $S_{i,\min}$ ($S_{i,\max}$). Furthermore we list the value of the significance of the signal including the interference for the parameter, where the significance of the interference is maximal (minimal) $S_{s+i}(x_{\min})$ and $S_{s+i}(x_{\max})$. The significance values are only approximate values obtained from the listed plots and were computed without including detector resolution effects.

Investigated parameters x	Other singlet parameter that differ from default scenario [a]	$S_{i,\min}$	$x_{\min}$	$S_{i,\max}$	$x_{\max}$	$S_{s+i}(x_{\min})$	$S_{s+i}(x_{\max})$	Obtained from Figure
$\phi \in [0, 2\pi]$	$g_{tt} = 0.66$	7.6σ	4.8	-7.6σ	0.6	7.9σ	-7.3σ	10
$m_s \in [500\,\text{GeV}, 950\,\text{GeV}]$	$\phi = \frac{\pi}{2}$, $g_{tt} = 0.26$, $g_{gg} = 2\frac{\alpha_s}{12\pi v}$	-6.0σ	550 GeV	-3.3σ	950 GeV	-5.8σ	-2.8σ	13
$\Gamma_s \in [5\,\text{GeV}, 195\,\text{GeV}]$	$\phi = 0$, $g_{tt} = 0.36$	7.6σ	4.8	-7.6σ	1.6	7.9σ	-7.3σ	18a
$\Gamma_s \in [5\,\text{GeV}, 195\,\text{GeV}]$	$\phi = 0$, $g_{tt} = 0.36$	-0.16σ	196 GeV	0.052σ	25 GeV	-0.16σ	0.12σ	18b
$g_{tt} \in [0.1, 0.73]$	$\phi = 0$	-0.02σ	0.28	0.11σ	0.56	-0.04σ	0.35σ	22a
$g_{tt} \in [0.1, 0.73]$	$\phi = \frac{\pi}{2}$	-8.4σ	0.73	-1.1σ	0.1	-7.1σ	-1.1σ	22b
$g_{gg} \in [\frac{\alpha_s}{12\pi v}$ [d], $0.001\,\frac{1}{\text{GeV}}]$	$\phi = 0$, $g_{tt} = 0.73$,	-0.1σ	$1.8 \times 10^{-5}\,\frac{1}{\text{GeV}}$	-18.6σ	$\frac{\alpha_s}{12\pi v}$	2839σ	-1σ	24a
$g_{gg} \in [\frac{\alpha_s}{12\pi v}$ [d], $0.001\,\frac{1}{\text{GeV}}]$	$\phi = \frac{\pi}{2}$, $g_{tt} = 0.73$	-771σ	$0.001\,\frac{1}{\text{GeV}}$	-8.4σ	$0.0008\,\frac{1}{\text{GeV}}$	3069σ	2839σ	24b
$\Gamma_s \in [5\,\text{GeV}, 145\,\text{GeV}]$, $g_{tt} = \sqrt{\frac{8\pi\Gamma_s 0.6}{\beta_q^3 3 m_s}}$	$\phi = \frac{\pi}{2}$, $\text{Br}(S \to \bar{t}t) = 60\%$	-8.3σ	$g_{tt} = 0.63$, $\Gamma_s = 15\,\text{GeV}$	-7.4σ	$g_{tt} = 1.96$, $\Gamma_s = 145\,\text{GeV}$	-7.8σ	-7.2σ	27
$m_q \in [4\,\text{GeV}, 172\,\text{GeV}]$	$\phi = \frac{\pi}{2}$, $g_{tt} = 0.45$	-5.9σ	135 GeV	-0.04σ	255 GeV	-5.7σ	-0.04σ	31

[a] Default parameter: $m_s = 500\,\text{GeV}$, $\Gamma_s = 20\,\text{GeV}$, $g_{gg} = \frac{\alpha_s}{12\pi v} = 9.91 \times 10^{-6}\,\frac{1}{\text{GeV}}$, $m_q = m_t = 172\,\text{GeV}$

Erklärung

Ich versichere, dass ich diese Arbeit selbstständig verfasst und keine anderen als die angegebenen Quellen und Hilfsmittel benutzt habe.

Heidelberg, den 28. September 2017,

Charlotte Neitzel